Genomic profiling and pre-clinical modelling of breast cancer leptomeningeal metastasis (BCLM) reveals acquisition of a lobular-like phenotype

Amanda Fitzpatrick[1,2], Marjan Iravani[1], Adam Mills[1], David Vicente[1], Thanussuyah Alaguthurai[3], Ioannis Roxanis[1], Nicholas C. Turner[1,4], Syed Haider[1], Andrew N.J. Tutt[1,3] and *Clare M. Isacke[1]

[1]The Breast Cancer Now Toby Robins Research Centre, The Institute of Cancer Research, London, UK.

[2]Comprehensive Cancer Centre, School of Cancer & Pharmaceutical Sciences, King's College London, UK

[3]Breast Cancer Now Research Unit, Guy's Hospital, King's College London, London, UK

[4]The Royal Marsden NHS Foundation Trust; London, UK

***Corresponding Author**: Clare M. Isacke, The Breast Cancer Now Toby Robins Research Centre, The Institute of Cancer Research, 237 Fulham Road, London SW3 6JB, UK. Telephone +44 20 7153 5510, Email clare.isacke@icr.ac.uk

Abstract

With a median survival of 4 months, the development of breast cancer leptomeningeal metastasis (BCLM) is devastating for patients. Investigating this often occult disease process is hampered by the difficulty of accessing leptomeningeal tumour material. Here, we utilise cerebrospinal fluid as a source of both cell-free DNA (cfDNA) and disseminated tumour cells, to explore the evolution of BCLM and heterogeneity between leptomeningeal and extracranial sites. CSF cfDNA sequencing detected actionable somatic alterations in 81% (17/21) of BCLM cases. Further genomic characterisation identified frequently altered genes involved in cell adherens junctions and cytoskeleton/chemotaxis pathways. Patient-derived organoids established from CSF tumour cells allowed profiling of this rarely available biological material, in addition to therapeutic testing and generation of *in vivo* models. Together these data reveal the development of BCLM is associated with the acquisition of a lobular-like breast cancer phenotype, and highlight potential approaches for tackling this hard-to-treat form of metastatic disease.

With advances in effective treatments for visceral metastasis, central nervous system (CNS) metastasis increasingly limit patient survival[1-3]. The development of leptomeningeal metastasis, where tumour cells spread over the lining of the brain and spinal cord and shed into the surrounding cerebrospinal fluid (CSF), is most commonly attributed to breast (35%), lung (25%), gastrointestinal (5%) and melanoma (5%) cancers[4]. Leptomeningeal metastasis causes debilitating neurological symptoms with often rapid clinical deterioration and a median survival of patients with BCLM of 3.4 – 5.4 months despite current treatments[5-11]. Published BCLM cohorts show enrichment for lobular breast cancer subtype[8,11,12], the most common 'special' subtype of breast cancer[13,14] which is defined histologically by the finding of discohesive tumour cells arranged in single files or as individual single cells[15], in contrast to the more common invasive carcinoma of no special type (IC-NST) which exist in nests or sheets of cells with preserved cell-cell adhesions[16].

In recent years there has been increased knowledge of the genetic events that evolve in metastatic breast and other solid cancers[17-23], however, the biology of leptomeningeal metastases remains poorly understood since the leptomeninges are a rarely-biopsied site and plasma liquid biopsies do not represent CNS-dominant cancers[24,25]. Gaining access to leptomeningeal tumour samples is key to answering fundamental questions about the cancer cell populations with intrinsic ability to enter and flourish in the CSF space.

Here we have utilised CSF sampling to both interrogate the genetics and evolution of BCLM via cfDNA sequencing from paired CSF and plasma, and generate preclinical *in vitro* and *in vivo* models of BCLM by the expansion of the rare CSF disseminated tumour cells (DTC). We demonstrate that BCLM shows early divergent evolution from the primary tumour and has a distinct genomic profile compared to other metastatic sites. Particularly noteworthy is the enrichment in BCLM of adherens junction and cytoskeletal/chemotactic alterations resulting in the acquisition of features and therapeutic vulnerabilities associated with lobular breast cancers. Together these findings illustrate a novel approach to translational research in BCLM integrating genomic and functional analytic methods, aiming to deliver improvements in patient care and survival.

Results

Comparative sequencing reveals unique genomic events in BCLM

It is often cited that BCLM is a late manifestation of widespread metastatic disease, however to date no studies have interrogated BCLM tumour evolution to determine the timing of BCLM seeding from primary tumour. Previously we described the prospective collection of CSF and plasma from a cohort of BCLM patients, and demonstrated the utility of using ultra-low pass whole genome sequencing (ulpWGS) to determine CSF circulating tumour DNA (ctDNA) content for BLCM diagnosis and therapy response monitoring[24]. Here we have investigated the genetic landscape of BLCM. A threshold of ≥10% tumour content was used to select liquid biopsy cfDNA samples for whole exome sequencing (WES). As previously reported[24,25], when metastatic disease is restricted to the CNS, ctDNA content in plasma is limited. Consequently although 21/21 of CSF cfDNA samples had sufficient tumour content only 11/21 paired plasma cfDNA samples were suitable for WES. WES was also performed on matched FFPE primary tumour (*n* = 18) and other available metastatic site samples (*n* = 8) (**Table 1; Supplementary Table 1; Fig. 1a, Supplementary Fig. 1a)**. Plasma-derived cfDNA was sequenced to a higher coverage (median 316x) than other samples (CSF cfDNA 164x, primary tumour DNA 195x, metastatic tumour biopsy DNA 211x) to account for the lower tumour content (median tumour content in plasma cfDNA 15.2% *vs*. CSF cfDNA 56.7%; **Supplementary Table 2; Supplementary Fig. 1b,c**).

To assess the inter-tumoral heterogeneity between BCLM (CSF cfDNA), extracranial metastases (plasma cfDNA or metastatic tissue) and the primary tumour, a multi-caller variant identification pipeline and post-hoc refinements approach was implemented to WES outputs to prioritise high-confidence variants (see Methods). Tumour mutational burden (TMB) across sample types was as expected for the breast cancer genome[26] with no significant difference between DNA source types (median CSF cfDNA 2.0, plasma cfDNA 2.0, primary tumour 1.3, metastasis 1.2 mutations/Mb, all ns by Mann-Whitney test) (**Supplementary Fig. 1d,e**). Indicative of a distinct genetic landscape in BCLM, 24.6% (IQR 14.3 - 42.6%) of cfDNA

mutations across CSF and plasma paired samples (*n* = 11) were unique to CSF, 16.8% (IQR 9.6 - 28.2%) were unique to plasma , and 43.4% (IQR 20.9 – 66.6%) were shared between both biofluids (**Fig. 1b**). There was no correlation between the proportion of unique variants in CSF *vs.* plasma and time to development of BCLM (time from primary tumour or metastatic diagnosis) nor to the number of previous treatment lines (**Supplementary Fig. 1f)**, indicating these factors do not account for the degree of variation between BCLM and extracranial disease. When examining single base substitution (SBS) signatures, a higher contribution of chemotherapy-related signatures (SBS11, SBS17b, SBS28, SBS31, SBS35, and SBS86) was found in plasma cfDNA compared to CSF cfDNA (median chemo-SBS contribution: 0.074 plasma; 0.043 CSF, $p = 0.033$) (**Fig. 1c; Supplementary Table 3**), likely reflecting the CNS 'sanctuary site' phenomenon, with lower exposure of BCLM to chemotherapy due to impedance by the blood-brain-barrier[27]. In keeping with published literature of the metastatic breast cancer mutational landscape[28], CSF cfDNA samples had higher SBS13 (APOBEC) signature contribution than primary tumours, and lower SBS1 (clock-like/FFPE artefact) and SBS23 (unknown aetiology) signatures (**Supplementary Table 3**).

Copy number variation (CNV) across the genome was determined using WES data including off-target (non-exome) reads (**Fig. 1d**), revealing common breast cancer events such as 1q and 8q gains, and 8p and 16q losses across samples[29]. Genetic loci with differentiating copy number status between CSF cfDNA and matched primary tumours or between CSF and matched plasma cfDNA samples were determined by comparing the rate of copy number events in each tissue type (**Fig. 1e**). Genes more commonly lost in CSF cfDNA compared to primary tumours included *PCDH9* and *PCDH17*, members of the cadherin superfamily, and *KLHL1*, an actin binding protein with a role in cytoskeleton reorganisation, with 16q regions containing the classical cadherin *CDH1* and other cadherins showing more frequent loss in CSF than plasma cfDNA samples. Gained regions in CSF cfDNA compared to plasma include 1q21.3 containing *TCHH* and *FLG2* (intermediate filament-associated proteins) and S100 family genes, implicated in poor prognosis breast cancer relapses[30]. Of note, in keeping with

findings in brain metastasis cohorts[31], *ERBB2* amplification in BCLM was a feature found to be shared with the primary tumour **(Fig. 2, Supplementary Fig. 2)**.

Cancer associated gene aberrations enriched in BCLM

To determine cancer-associated genetic aberrations enriched in BCLM compared to other non-BCLM metastatic breast cancer samples, the alteration rate (including high level copy number events, and mutations) of the 36 most frequently BCLM-altered cancer genes identified by WES was compared to a publicly available sequencing dataset of 216 non-BCLM metastatic breast cancer samples[32] (herein known as MBC cohort) (**Fig. 2; Supplementary Fig. 2)**. The following 10 genes (highlighted in red on panels) displayed significantly different alteration rate in BCLM compared to the MBC cohort; *CDH1, MUC16, TBX3, ARHGEF10, MDM2, WRN, CTNNA1, NUTM2A, PSIP1* and *MLH1* ($p \leq 0.05$, Chi-square test) (**Supplementary Table 4**).

Due to enrichment for lobular breast cancers in our BCLM cohort **(Table 1, Supplementary Table 1)** the high rate of *CDH1* (E-cadherin) mutations (52%) was an expected finding, since deleterious *CDH1* mutation occurs in the majority of invasive lobular breast cancers (ILC) leading to the characteristic discohesive lobular phenotype[33,34]. In contrast to lobular cancers, *CDH1* mutations are rare in IC-NST (2.3% of 780 invasive ductal carcinoma (IDC)/IC-NST; Breast Invasive Carcinoma TCGA data). CTNNA1 (α-catenin) plays an indispensable role in forming functional adherens junctions by linking the cadherin/β-catenin complex to the underlying actin cytoskeleton[35]. Although *CTNNA1* mutations and copy number aberrations are rare in both primary ILC and IC-NST (0.5% of 201 ILC, 1.5% of 780 IDC/IC-NST; Breast Invasive Carcinoma TCGA data), loss of *CTNNA1* has been demonstrated to lead to a lobular morphology in pre-clinical models[36].

We identified both *CDH1* and *CTNNA1* deleterious alterations in BCLM occurring in non-lobular cases, and often as BCLM-private events, implying that adherens junction defects are important drivers of BCLM biology **(Fig. 2; Supplementary Fig. 2)**. Unexpectedly for breast cancer of apocrine morphology (**Table 1**), KCL617 displayed a frameshift *CDH1* mutation in both primary tumour and CSF cfDNA, with *CDH1* loss of heterozygosity (LOH) acquired in the CSF cfDNA; while CSF cfDNA from KCL566 (IC-NST) harboured a stop-gain *CDH1* mutation plus *CDH1* LOH, with neither aberration being detected in the matched samples **(Fig. 2; Supplementary Fig. 2)**. KCL622 and KCL625 (both IC-NST) displayed *CTNNA1* homozygous deletions in CSF cfDNA, with *CTNNA1* copy number neutral status in matched primary tumours. KCL658 (IC-NST) displayed a *CTNNA1* stop-gain mutation in both CSF cfDNA and the matched plasma cfDNA and KCL650 (IC-NST) displayed *CTNNA1* homozygous deletion in CSF cfDNA, with heterozygous loss in the plasma cfDNA, in both these cases no primary tumour was available for sequencing **(Fig. 2; Supplementary Fig. 2)**. *CTNNA1 and CDH1* aberrations displayed mutually exclusivity in BCLM samples (**Fig. 2; Supplementary Fig. 2**).

Finally, a member of the RhoGEF family, *ARHGEF10* which displayed a low aberration rate in the MBC cohort (3.2%), was highly aberrated in BCLM CSF cfDNA (23% of cases), comprising four homozygous deletions and one BCLM-unique missense mutation. Further to this, nine samples demonstrated *ARHGEF10* heterozygous losses **(Fig. 2; Supplementary Fig. 2)**. *ARHGEF10* facilitates activation of Rho[37] and downstream Rho kinase (ROCK) to promote actomyosin contractility. Excessive actomyosin contractility has been reported to impair adhesion to, and migration on, collagen I and is deleterious to ILC development[38-40], consequently it is tempting to speculate that loss of *ARGHEF10* provides a pro-survival mechanism for BCLM.

Biological pathway analysis shows enrichment for cytoskeletal aberrations in BCLM

The ability of tumour cells to gain access to the leptomeningeal space via the blood-brain/blood-CSF-barrier, and successfully interact with the unique microenvironment in this

space, may require genetic alterations not currently characterised as cancer-driver genes. To assess non-cancer gene alterations acquired in BCLM *vs*. extracranial metastases, we performed gene set enrichment analysis of frequently altered (by mutation, amplification or deletion) genes in CSF (n = 257) and plasma (n = 160) cfDNA (**Fig. 3a,b; Supplementary Fig. 3**). CSF and plasma cfDNA samples shared alterations in genes involved in 'endomembrane system organisation', and 'fibroblast growth factor response'. By contrast, GO terms showing enrichment in CSF compared to plasma cfDNA were; 'positive chemotaxis', 'myelination' and 'supramolecular fiber organization', the latter encompassing key cytoskeletal scaffold components (actin filaments, intermediate filaments and microtubules) and their regulators. Within the 'supramolecular fiber organization', *CTNNA1, MYO15A, DMTN and SPTA1* (**Fig. 3b**) are of interest. α-catenin (*CTNNA1*) alterations, as discussed above, are associated with the acquisition of a discohesive, 'lobular-like' phenotype[36,41]. Myosin 15A (*MYO15A)*, an actin-based motor molecule was frequently aberrated in CSF cfDNA samples 6/21 (29%), with stop-gain and missense variants predominating and often accompanied by loss-of-heterozygosity (LOH). Dematin actin binding protein (*DMTN*), a regulator of cytoskeleton remodelling[42,43] displayed homozygous deletion in 3/21 CSF cfDNA samples and deleterious frameshift and missense mutation in a further 3/21 samples, and these aberrations were more often BCLM-private (**Fig. 3b**). Spectrin-alpha 1 (*SPTA1*), a scaffold protein linking the plasma membrane to the actin cytoskeleton, was commonly aberrated in BCLM CSF cfDNA samples by missense variants (4/21) and amplification (2/21) (**Fig. 3b**). Within 'myelination', CSF cfDNA samples were enriched for genetic alterations in *ARGHEF10* (discussed above), and genes with role in cell-cell adhesion including neurofascin *(NFASC)* and teneurin transmembrane protein 4 (*TENM4*). Within 'positive chemotaxis', amplifications were found in scribble planar cell polarity protein (*SCRIB*), previously demonstrated to promote cell migration and metastasis[44-46]. Genomic alteration in beta-defensin proteins (*DEFB4A, DEFB103B, DEFB104B*) were also enriched in BCLM samples (**Fig. 3b**). Beta-defensins are antimicrobial peptides with multiple suggested functions in cancer cells including regulation of migration[47]. Taken together, these findings imply that regulation of cell-cell

adhesion, cell cytoskeleton, motility and migration may be key to dissemination of tumour cells to the leptomeninges and their survival in this metastatic niche.

BCLM subclones seed early during primary tumour evolution

To investigate the evolution of BCLM, mutational allele frequencies were used to infer phylogenetic evolution (**Fig. 3c; Supplementary Fig. 4**). These analyses revealed (a) rather than a late-metastatic seeding event, BCLM disseminates early from the primary tumour, (b) CSF and plasma cfDNA display divergent evolution, often sharing branches with other metastatic sites but possessing distinct mutational repertoires, and (c) in 4/21 cases a variant with proven or predicted actionability was present in CSF cfDNA which was not present in the primary tumour; a *BRCA2* frameshift mutation p.N1599Ifs*18 accompanied by LOH in KCL610 predictive of response to PARP inhibitors, and a mono-allelic *BRCA1* frameshift mutation p.Y655Vfs*18 in KCL148 which may predict response to PARP inhibitors; an *NF1* frameshift mutation p.Y1586Ifs*17 in a late BCLM-subclone of KCL566 potentially targetable by MEK inhibition, and an *ESR1* p.Y537 mutation private to KCL680 BCLM subclones and predictive of a loss of response to aromatase inhibitor but retaining sensitivity to the oestrogen receptor degrader, fulvestrant. Furthermore, two CSF samples, KCL566 and KCL148, exhibited high TMB (>10 mutations/Mb) **(Fig. 2)** predictive of response to immune checkpoint inhibition. It was noted that both these TMB-high cases had truncal *MLH1* aberration however substantial elevation of TMB was seen in CSF cfDNA compared to matched tissues indicating further accumulation of mutational events in the leptomeninges (**Supplementary Fig. 1e**).

Including actionable variants acquired in the BCLM subclones, alterations with potential actionability were discovered 17/21 (81%) BCLM cases by CSF cfDNA sequencing, with OncoKB therapeutic level 1 alterations in 12/21 (57%) (**Fig 3c**, and **Supplementary Fig. 4**, actionable variants highlighted green; **Supplementary Table 5)**. Those occurring in more than 1 case being *ARID1A* deleterious mutations in 3 cases, *PIK3CA* activating mutations in 5 cases, *PTEN* deleterious mutations in 2 cases and *MDM2* amplifications in 3 cases. Although

this reveals the potential for improved targeting of BCLM using therapy tailored to identified genomic aberrations, an important caveat is the uncertainty of drug penetration through the blood-brain/blood-CSF-barrier to reach therapeutic concentrations within the CSF.

Development and characterisation of BCLM PDOs

A major challenge in investigating the biology of BCLM is the lack of access to clinical biopsies. To overcome this challenge, we developed methodologies for *in vitro* expansion of the small number of viable DTCs present in CSF samples, resulting in the successful development of 5 BCLM PDOs (**Fig. 4a**). Following WES, comparison of copy number profiles between the BCLM PDOs and their matched CSF cfDNA samples revealed high level concordance (Pearson correlation coefficients from 0.808-0.965; **Fig. 4b** upper panel) while comparison of the mutational landscape revealed a median of 81.5% of CSF cfDNA detected variants present in BCLM PDOs (**Fig. 4b** lower panel). The high concordance between CSF cfDNA and CSF derived tumour cell DNA, confirms that CSF cfDNA represents a valid surrogate for the rarely available BCLM genetic and biological material.

Consistent with genomic analysis of CSF cfDNA (**Fig. 1-3**), immunohistochemical staining (**Fig. 4a**) and transcriptional profiling (**Fig. 4c**) of the PDOs and matched primary tumours (**Table 1**) reveals a loss of E-cadherin staining and reduced *CDH1* expression in PDO KCL566 (IC-NST with acquired *CDH1* truncating mutation in CSF cfDNA) and the loss of membrane associated α-catenin staining and reduced *CTNNA1* expression in PDO KCL622 and PDO KCL625 (both IC-NST showing acquired *CTNNA1* homozygous deletion in CSF cfDNA). p120-catenin cytoplasmic location is a hallmark of classical ILC[48], and was observed in the primary and PDO KCL320 (ILC) and KCL450 (ILC). By contrast, PDO KCL566 showed mixed cytosolic and membranous p120-catenin and PDOs KCL622 and KCL625 showed membranous p120-catenin (**Fig. 4a**). These findings agree with published reports, that *CTNNA1* loss in the presence of *CDH1* expression, does not lead to p120-catenin cytosolic

localisation despite *CTNNA1* deficient cells acquiring 'lobular-like' features of a rounded cell morphology and anoikis resistance[36].

Also notable was the loss of ER expression in the 3 PDOs derived from patients with ER+ primary tumours (KCL450, KCL566, KCL320) (**Fig. 4a; Supplementary Table 6**). Although loss of ER expression is reported to occur in ~25% of PDO derivations[49], reduced ER expression in metastatic site tissue of ER+ primary breast cancers is also reported[50-52] and is linked to more frequent *TP53* mutation in metastases[53]. Our BCLM samples showed higher rates of *TP53* mutation and copy number loss CSF cfDNA (12/21) than the primary tumour (6/18) (**Supplementary Fig. 2**), which could explain frequent ER expression loss. Of note, there was a relative lack of *ESR1* mutations detected in CSF cfDNA (1/21), despite fourteen patients having previously received aromatase inhibitor therapy (**Supplementary Table 1**). This may reflect the mutual exclusivity of *TP53* and *ESR1* mutations in metastatic breast cancer[53].

Finally, immunohistochemical staining revealed acquisition of HER2/ERBB2 expression in 4/5 PDO (ranging from 1+ to 3+ on IHC scoring), in all cases the matched primary tumours were HER2-negative (**Fig. 4a; Supplementary Table 6**). We did not identify copy number level changes in *ERBB2* (**Fig. 2; Supplementary Fig. 2)**, in agreement with published cohorts in breast cancer brain metastasis which show increased *ERBB2* expression in brain metastases compared to their matched primary tumours[54-56]. The acquisition of HER2 expression in non-amplified cancers (HER2-low) has therapeutic implications given CNS disease response to HER2-antibody-drug-conjugates (HER2-ADCs)[57,58].

Patient-derived xenograft models reveal distinct BCLM organotropism

Although informative, to date models of BCLM have been limited to selecting non-BCLM-derived breast cancer cell lines for their ability to grow in the leptomeninges[59]. To study the organotropism of CSF DTC-derived PDOs, PDOs were transduced to express mCherry and

luciferase 2 (mChLuc2) (**Supplementary Fig. 5**) prior to inoculation into immunocompromised mice. Orthotopic inoculation into the mammary fat pad revealed a variable ability of BCLM PDOs to form primary breast tumour xenografts (**Fig. 5a**). For PDOs KCL320 and KCL450 only small tumour masses were detectable in a subset of inoculated animals, with no evidence of spontaneous metastasis to secondary sites. Of note, these PDOs were derived from the two patients with Luminal A, de-novo ILCs (KCL320 and KCL450). By contrast, PDOs KCL566, 622 and 625) readily formed primary tumours with KCL566 and KCL622 showing widespread spontaneous metastasis including, in a subset of mice, to the leptomeninges. Of note PDO KCL566 displayed loss of E-cadherin, in keeping with the *CDH1* truncating mutation acquired in the CSF cfDNA sample from this ductal adenocarcinoma (see **Fig. 4a**). PDO KCL320 is of interest as it is derived from CSF DTCs of a patient with metastatic disease restricted to the leptomeninges, and *in vivo* showed preference for growth in the CNS environment. In addition to its failure to grow robustly after orthotopic inoculation (**Fig. 5a**), PDO KCL320 did not grow following intraductal inoculation into the mouse mammary gland (MIND model) (**Fig. 5b**) or by intraperitoneal inoculation (**Fig. 5c**). However, following intracardiac inoculation, 4 out of 5 BCLM PDOs (including PDO KCL320) resulted in colonisation of the leptomeninges and the brain parenchyma in 100% of mice (**Fig. 6a**). Intracerebroventricular (ICV) inoculation of KCL320 PDO directly into the CSF resulted in metastatic disease restricted to the leptomeninges (**Fig.6b**). In addition to the leptomeninges, BCLM PDOs display a strong predilection for metastasising to endocrine organs such as the ovaries, adrenal glands and pituitary gland, a feature associated with the metastatic spread of ILC[60]. Moreover, this pattern of metastatic spread in the mice is distinct from the metastatic involvement in the patients from whom the PDO cohort was derived, with only 1/5 patients (KCL625) recorded as having metastatic disease in endocrine tissues (**Table 1**). This endocrine tissue organotropism likely reflects the high rate of mutation in E-cadherin or the associated junctional component α-catenin in BCLM CSF samples, even in those arising from primary IDC-NST carcinomas, suggesting that colonisation of the leptomeninges strongly selects for ILCs or breast cancers with lobular-like features. Consequently, we next assessed

the responsiveness of the BCLM PDOs to standard of care drugs and drugs identified to show selectivity for lobular breast cancer.

Therapeutic targeting of BCLM PDOs

The standard-of-care treatment approach for patients with LM is delivery of methotrexate into CSF, via repeated lumbar puncture or an intraventricular device such as an Ommaya reservoir, however randomised trial evidence for its effectiveness is lacking. Compared to a breast cancer cell line (DU4475, grown in 3D spheroids in PDO culture conditions) which shows complete response to methotrexate, PDO KCL622 shows no response and the remaining 4 BCLM PDOs show only a partial response despite the high drug concentrations used (**Fig. 7**, upper panels).

Due to the enrichment for cell-cell adhesion defects in this cohort of BCLM cases, we explored a potential therapeutic approach of receptor tyrosine kinase ROS proto-oncogene 1 (*ROS1)* inhibition[61], currently under investigation in *CDH1*-defective tumours in a Phase II trial (ClinicalTrials.gov NCT03620643). 3D *in vitro* therapeutic responses were assessed in BCLM PDOs using crizotinib (**Fig. 7**, middle panels) and the blood-brain-barrier penetrant ROS1 inhibitor taletrectinib (**Fig. 7**, lower panels). Compared to MDA-MB-134-VI cells (*CDH1*-defective, ILC cell line used as positive control) and T47-D (CDH1-proficient, IC-NST cell line used as a negative control), 4/5 BCLM PDOs displayed reduced survival upon ROS1 inhibition, with the most sensitive being PDO KCL622 (IC-NST, *CTNNA1* deletion unique to BCLM) and PDO KCL566 (IC-NST, *CDH1* truncating mutation unique to BCLM).

Discussion

Recent studies in metastatic breast and other solid tumours[17-23], have demonstrated specific genetic alterations in metastases beyond those observed in primary tumours. However, to date, metastasis to the leptomeninges has been relatively unstudied due to difficulty accessing material from this rarely biopsied site. Here we present genetic profiling of a cohort of BCLM samples (both CSF cfDNA and CSF-DTCs expanded in culture as PDOs) with concurrently sequenced plasma cfDNA and archival tumour tissues, allowing comparison of BCLM with the primary tumour and extracranial metastatic sites. Echoing the findings of the above studies, and of Brastianos and colleagues in the setting of parenchymal brain metastases[62] we found that BCLMs possess unique mutations which could not be detected in the primary tumour, suggesting they existed as rare subclones in the primary that had acquired biological features selected for during tropism to the BCLM niche and/or arose through further genetic evolution within this niche. The added value of our study was concurrent sequencing of plasma cfDNA and/or extracranial metastasis (13/21 cases) revealing divergent subclone evolution between the CSF and plasma compartments, further highlighting that metastases spatially separated by the blood-brain/blood-CSF-barrier bear distinct molecular changes not only from the bulk of the primary but also from those in extracranial metastatic niches. These alterations could be hypothesised to confer specific BCLM niche-specific biological attributes. It was also revealed that leptomeningeal and extracranial metastases have different evolutionary pressures, with plasma cfDNA bearing increased marks from previous chemotherapy treatment, implying that the blood-brain/blood-CSF-barrier may effectively create a sanctuary to CNS disease. We show that sequencing CSF cfDNA uncovers additional genetic alterations with predicted or potential actionability over primary tumour sequencing alone, supporting the use in BCLM of CSF liquid biopsy for precision medicine approaches, albeit with the caveat that many novel systemically-delivered agents have not been assessed for their blood-brain/blood-CSF-barrier penetration and CNS responses. Further, CSF-DTCs expanded in culture allowed assessment of BCLM transcriptional level alterations, and revealed receptor subtype switches between the primary tumour and matched PDO. This opens potential new

therapeutic opportunities for BCLM in hitherto HER2-negative cases, for example using systemically-delivered HER-ADCs to target gains in HER2 expression, which are shown to be effective in HER2-amplified and HER2-low brain metastases, with trials ongoing in BCLM[57,58]. The gain in HER2 expression in BCLM vs. primary tumour, and loss of ER expression, highlights the need for integration of BCLM receptor subtype assessment into clinical practice; which could be achieved by techniques such as immunomagnetic CTC capture[63].

A striking insight to BCLM biology was the enrichment for alteration of genes involved in cell-cell adhesion, cytoskeletal regulation, chemotaxis and cell migration. It is well established that ILCs have a distinct biology, defined by a lack of cell-cell adhesion as a result of inactivation of *CDH1*, displaying a discohesive and highly migratory phenotype[64-66] and display metastatic site predilection to leptomeninges and other fluid-filled serosal-lined cavities including peritoneum, pleural and pericardial spaces[67]. We found that BCLM samples, whether derived from ILC or non-lobular primary tumours, were enriched for alterations in *CDH1*. In addition, we identified *CTNNA1* and *ARHGEF10* loss-of-function alterations, preferentially in BCLM derived from non-ILC tumours. *CTNNA1* is a key component of the adherens junction, and although not frequently altered in breast cancer, *in vitro* studies have shown that *CTNNA1* loss leads to a lobular-like morphology[36]. *ARHGEF10* is a GTP exchange factor for RhoGTPases, and *in vitro* studies have demonstrated increased cell motility and invasiveness in *ARHGEF10* depleted PDAC cells[68]. We propose that *CTNNA1* and *ARHGEF10* defects may be an alternative mechanism to become 'lobular-like' and lead to a biological predilection for leptomeningeal colonisation. To successfully grow in the leptomeningeal microenvironment, tumour cells must overcome challenges posed by the unique fluid-filled, nutrient-poor microenvironment. Others have demonstrated that ILC cells display anchorage-independent growth and anoikis resistance through increased levels of Rho/ROCK signalling mediated by the translocation of p120-catenin to the cytosol[48,66]. In the nutrient-sparse CSF[69], cells will have a survival advantage if they can enter a dormant, anoikis-resistant state via sustained G0/G1 cell cycle arrest[70] until they adapt to the harsh environment and re-enter proliferation.

In support of BCLM cells displaying a 'lobular-like' biology, *in vivo* models of tumour dissemination via haematogenous route, showed BCLM cells had a predilection for growth in the ovaries, and pituitary and adrenal glands, at higher rates than in the patients these derived from. This suggests that the biological adaptation which BCLM tumour cells undergo in the leptomeningeal space, confer an advantage to growth in endocrine organs[60], reflecting their shift to a more 'lobular-like' phenotype through the adherens junction and cytoskeletal defects.

Advances in the treatment of BCLM and leptomeningeal metastasis from other solid tumours are desperately needed. The standard-of-care BCLM intrathecal agent, methotrexate, was not particularly effective in BCLM PDOs treated *in vitro*, despite being used at concentrations similar to that achieved by intra-CSF injection. Although originally investigated in the adjuvant setting, methotrexate is not a commonly used chemotherapeutic agent in breast cancer, and the only randomised trial of intrathecal methotrexate in BCLM, failed to show a significant improvement in survival using this treatment[71]. Given the pressing requirement to discover novel approaches to treat BCLM, we describe the potential of CSF sampling and subsequent PDO derivation to enable discovery and functional validation of actionable targets. The genomic findings also highlight the potential clinical value of CSF cfDNA profiling for patients affected by this condition, and support the notion that BCLM may be better treated by discovery of blood-brain/blood-CSF-barrier penetrant therapies rather than intrathecal cytotoxic chemotherapy. Importantly, the identification of cell-cell adhesion and cytoskeleton alterations both provides insight to the biology of BCLM and its ability to flourish in this metastatic site, but also presents a potential 'Achilles-heel' for therapeutic targeting, such as ROS1 inhibition[61] and other emerging approaches[72,73]. The methodologies and novel models described here will serve as an important resource for the ongoing research into leptomeningeal metastasis with the overarching aim to improve therapeutic options and patient survival.

Funding

This study was supported by: Medical Research Council Clinical Research Training Fellowship - MR/P001564/1 (AF, CI), NIHR Biomedical Research Centre (BRC) at the Royal Marsden and the ICR post-doctoral support funding- W94500 (AF), Breast Cancer Now Programme Funding to the Breast Cancer Now Toby Robins Research Centre - CTR-Q4-Y1-5, CTR-Q5-Y1 (CI, NT, AT) and to the Breast Cancer Now Research Unit at Kings College London - KCL-Q2-Y1-5, KCL-Q3-Y1 (AT), Cancer Research UK Centre Grant funding to the Kings College London - CRUK RE15196-9 (AT).

Author Contributions

Conceptualization AF, ANJT, CMI

Supervision SH, ANJT, CMI

Funding acquisition AF, ANJT, CMI

Investigation AF, MI, AM, DV, TA, IR, NCT, SH, ANJT, CMI

Writing - original draft AF, MI, ANJT, CMI

Writing - review and editing AF, MI, AM, DV, TA, IR, NCT, SH, ANJT, CMI

Acknowledgements

We would like to thank Naomi Guppy and her team in the Breast Cancer Now Toby Robins Research Centre Nina Barough Pathology Core Faculty for histopathology support and the following facilities at the ICR; Tumour Profiling Unit, Biological Services Unit, FACS and Light Microscopy Facility. We thank Eleanor Knight, Daniela Nova and Rebecca Marlow in the Breast Cancer Now Toby Robins Research Centre Patient Derived Models facility for their help in establishing the PDO culture methodologies and OcellO for providing the PDO medium. We thank John Alexander, Erle Holgersen and Hui Xiao in Syed Haider's team for their contributions to data analysis. We thank Phil Bland (ICR) for mouse intraductal injections. For patient enrolment and sample collection at Kings College London and Guys and St Thomas's NHS Foundation Trust, we thank clinicians S. Irshad, H. Kristeleit, J. Mansi, M.

Nathan, E. Sawyer, A. Swampillai, M. Harries and the study nurses and staff, and R. Liccardo, R. Marlow, and V. Shah for patient enrolment and sample preparation collection. For patient enrolment and sample collection in Royal Marsden NHS Foundation Trust, we thank clinicians S. Johnston, M. Parton, M. Robert, L. Ulrich and A. Okines and the study nurses and staff, A. Bambra, D. Kelly, S. Thompson.

Competing Interests statement

The authors have no conflicts of interest to declare

Methods

Patients and clinical sample collection

CSF and blood were concurrently collected from breast cancer patients at initial evaluation of BCLM (*n*=21) as previously described[24]. Archived primary tumour and any metastatic recurrence tissues were retrieved. Written informed consent was obtained from all individuals in accordance with the Declaration of Helsinki under the following research ethics committee approved studies (REC ID 13/LO/1248, South East London Cancer Research Network, UK, and REC ID 14/LO/0292, Royal Marsden NHS Foundation Trust, UK). Histological subtype of primary tumours and BCLM PDOs were classified by independent breast pathologist review (I.R.).

Sample handing and processing

CSF samples were collected in standard universal containers and stored transported on wet ice to the laboratory, for centrifugation within 1 hour of collection at 300*g* for 10 minutes. CSF supernatant was stored at -80°C. The resultant CSF cell pellet was used for immediate entry to organoid culture (see below) or cells were re-suspended in 100 µL of 20% DMSO/FBS plus 100 µL OcellO primary organoid media, and frozen to -80°C at a cooling rate of -1°C per minute using a Nalgene Cryogenic Freezing container. Extraction of CSF and plasma cfDNA, extraction of DNA from germline (buffy layer) and archival tissues, and ulpWGS for tumour purity assessment of cfDNA, has been previously described[24]. DNA from BCLM PDOs was extracted using Qiagen Blood and Tissue Kit.

Whole exome sequencing (WES)

Germline, tumour tissue and organoid DNA were fragmented to 200 base pair (bp) length using a Covaris E Series instrument (Covaris, MA, USA), while cfDNA was not further fragmented. Sequencing libraries were made using SureSelect XT Low Input Library Preparation kit and Agilent Bravo Automated Liquid Handling Platform. SureSelect XT Low

Input Dual Index P5 Indexed Adaptors were used for cfDNA to minimise index hopping [74]. Number of pre-capture PCR cycles was 8 - 14 based on input DNA quantity and quality (assessed by Agilent TapeStation) as advised by the manufacturers' protocol, and run on an AB Veriti 96-well Thermocycler (Applied Biosystems, CA, USA). The target amount for hybridisation was 1000 ng. Exome capture was performed using the SureSelect XT Low Input Target Enrichment kit, Dynabeads MyOne Streptavidin T1 magnetic beads and the SureSelect XT Low Input Human All Exome V6 panel (60 Mb). The resultant libraries were run on the NovaSeq 6000 with an S2 flowcell (Illumina, San Diego, CA, USA) acquiring 2 × 100 bp paired-end reads. WES analysis was run through a bespoke pipeline using Nextflow v20.10.0 (doi:10.1038/nbt.3820). Further analysis and plotting were performed in R 3.6.0.

(1) Alignment, duplicate removal and quality control: Reads from exome sequencing FASTQ files were first trimmed with Trim Galore v0.6.6 (https://github.com/FelixKrueger/TrimGalore), a wrapper script for Cutadapt (https://doi.org/10.14806/ej.17.1.200) and FastQC (https://qubeshub.org/resources/fastqc). Reads were then aligned against the human assembly build GRCh38 using Burrows-Wheeler Aligner (BWA) mem v0.7.17, run with default settings. Duplicate reads were removed with Picard Tools v2.23.8 according to Genome Analysis Toolkit (GATK) Best Practices recommendations[75]. GATK v4.1.9.0[76] was used for base score recalibration. Sample coverage statistics were calculated with the CollectHsMetrics command in Picard. Coverage is displayed in **Supplementary Fig. 1c** and **Supplementary Table 2**. NGSCheckMate (downloaded March 15th 2018, commit number 1079908) was run to check for concordance between tumour and normal pairs for all patients, thus verifying sample identity[77].

(2) Variant calling: A consensus variant calling method was used that included four variant callers: MuTect2[78], MuSE[79], LoFreq[80], and Strelka[81].

MuTect2: Before variant calling, a panel of normals was created by running MuTect2 (embedded in GATK v4.1.9.0) in unpaired mode on all germline samples in the study and aggregating the results with the CreateSomaticPanelOfNormals command. Paired tumour/germline variant calling was performed with MuTect2, which was provided with both the panel of normals and the Genome Aggregation Database (gnomAD) v3.1 for filtering. Resulting variants were further filtered on contamination fractions and orientation biases with the FilterMutectCalls command. Only biallelic calls were retained for further processing. Variants were annotated with ANNOVAR (2016-02-01 version)[82]. PolyPhen-2[83] and SIFT[84] algorithms, embedded in ANNOVAR, were used for predicting the effects of non-synonymous variants on protein function.

MuSE: MuSE was run in exome mode on the tumour-germline pairs. The gnomAD database was provided for removal of common variants.

LoFreq: Tumour and germline BAM files were first run through LoFreq's indelqual command to add the required information for calling indels. Then the somatic command was used to perform the variant calling. The gnomAD database was once again used as a resource of common variants.

Manta and Strelka: Manta and Strelka were run, in that order, to perform indel calling and SNV calling, respectively. Both were restricted to the exome. Indel and SNV data were combined at the end of the run.

The resulting variants were merged and restricted to only those reported by two or more callers. Those variants were further filtered; (a) by limiting them to exonic or splicing regions and (b) by applying a set of quality filters as follows: a minimum of 5 supporting reads in the tumour sample, a maximum of 2 reads in the germline sample, a minimum coverage depth of 10 reads, and a minimum VAF threshold (as defined below). The two exceptions to this were low coverage (median coverage ≤50x) samples (CSF samples RMH010, RMH011 and

KCL680) that had reduced read thresholds of 3, 1, and 7, respectively, and LoFreq variants for which the number of supporting reads in the normal sample is not reported. (c) A higher threshold was applied in each purity stratum to C>T and G>A variants to remove FFPE artefacts and (d), in cases where a variant passed these filters in one tissue of a patient but not in another, the non-passing variant call was exempted from the filtering due to the additional evidence. Tumour mutational burden (TMB) was calculated for each sample by dividing the total number of these variants by the total megabases covered by the exome target panel.

Tumour purity and ploidy estimates were obtained from PureCN v1.16.0[85] except in the following situations (a) cfDNA samples, which had also undergone ulpWGS, where difference between PureCN and ulpWGS purity estimate >± 0.15, (b) samples with PureCN ploidy >3.5 or <1.5, (c) tumour tissue DNA with purity estimate ≤0.35. For these samples, manual curation of purity and ploidy was performed to reach a consensus purity and ploidy estimate, by examining the ichorCNA and CNVkit copy number profiles, and the median VAF of somatic variants present in the sample.

High purity samples (purity >0.5) were subjected to the highest filtering thresholds of 0.05 minimum VAF for non-FFPE samples and 0.07 minimum VAF for C>T and G>A SNVs in FFPE samples. For low purity samples (purity ≤0.2), the minimum VAF filters were adjusted to 0.01 (non-FFPE) and 0.03 (FFPE). For samples with purities between 0.2 and 0.5, intermediate VAF thresholds were set to 0.03 (non-FFPE) and 0.05 (FFPE).

<u>(3) Mutational signatures analysis</u>: Consensus variant calls from each sample were converted back into VCF format using the MutationalPatterns R package[86]. Cosine similarity and signature contribution were calculated based on the COSMIC SBS signatures v3.2[87].

(4) Cancer-associated gene lists (used in **Fig. 2 and Supplementary Fig. 2**). Cancer Gene Census list[88] was downloaded from COSMIC database (https://cancer.sanger.ac.uk/census) on 4th July 2018 (719 genes). Breast cancer driver gene list (89 genes) was created by combining breast cancer drivers identified in two published studies[89,90]. OncoKB actionable variants (Therapeutic Level 1 - 4) were identified by accessing https://www.oncokb.org on 17th February 2022.

(5) Copy number alteration calling: Copy number $\log_2$ ratios were obtained from CNVkit v0.9.9[91], with each tumour sample run against a normal reference built from all matched germline samples in the study. The segmented ratios from each sample were then adjusted for tumour purity and ploidy, which were determined as described above. A copy number ratio was assigned to each gene using CNVkit's genemetrics function. To call copy number states, $\log_2$ ratios were first standardised (normalised to standard deviation) within each sample and copy number states were called for each sample as follows:

Genes with a standardised $\log_2$ ratio (z) were assigned copy number states as follows: amplification >2.0; gain >1.0 to ≤2; deletion <-2.5; loss <-1.5 to ≤2.5; neutral copy number state ≥-1.5 to ≤1.0.

For CNV proportion test, differences in copy number state between tissue types were analysed with two-sided tests of equal proportions in R. Separately, GATK v4.1.9.0 haplotype caller was run on both tumour and normal samples to obtain B-allele frequencies. ASCAT v2.5.1[92] was provided with the same purity and ploidy estimates used with CNVkit. and used to obtain allele-specific copy number calls for use in PyClone (see below).

(6) Genetic alterations in BCLM *vs*. metastatic breast cancer (MBC) cohort. Mutation and copy number data from a cohort of 216 MBC samples which had undergone WES biopsy in the context of the SAFIR01 and SAFIR02 prospective trials[32]

(https://www.cbioportal.org/study/summary?id=brca_igr_2015; downloaded 9th August 2022). Rate of genetic alteration (including mutation, amplification and deletion) in each cohort (BCLM *vs.* MBC) were compared by proportion Chi-square test, using R.

(7). Gene set enrichment analysis: Genes enriched for alterations (including mutation, amplification and deletion) *vs.* matched primary tumour, 257 genes in CSF (altered in ≥4/21 of CSF samples and ≤2/21 matched archival tissue samples) and 160 genes in plasma (altered in ≥3/11 plasma samples and ≤2/21 matched archival tissues) were used as input lists for statistical overrepresentation test using the GO Biological Process (complete) annotation set of PANTHER database (http://www.pantherdb.org, analysis performed 12th July 2022). Enriched gene sets were retained if $-\log_{10}$ p-value (Fisher's exact test) was ≥3.0 in either CSF or plasma list, and if the reference list (size of GO family) was ≥10.

(8) Subclonal reconstruction and clonal evolution modelling: Subclonal reconstruction was performed with PyClone v0.13.1[93]. Variant clusters with corresponding cellular prevalence identified by PyClone were used as input to ClonEvol (Version 0.99.11)[94] run in R for clonal ordering and phylogenetic tree construction. Unless otherwise stated, analysis parameters were: number of mutations per cluster ≥10; cluster VAF of >0.05; monoclonal cancer initiation model; bootstrap, non-parametric subclonal test with a minimum probability that cluster is non-negative with a p-value set at 0.05.

RNAseq analysis of primary tumour and matched BCLM PDOs

Total RNA from archival primary tumours (FFPE) was extracted by AllPrep DNA/RNA FFPE Kit following macrodissection of involved tumour areas. Cell lines and early passage (passage number 3 - 5) PDOs were harvested in RLT buffer upon establishment of organoids (8 - 16 days post seeding), and total RNA extracted using the RNeasy kit (QIAGEN) according to the manufacturer's instructions. RNA samples were quantified using Qubit 2.0 Fluorometer and RNA integrity was checked with Agilent TapeStation. RNA from PDOs underwent library

preparation using NEBNext Ultra RNA Library Prep Kit for Illumina and sequenced on Illumina HiSeq acquiring paired end reads. RNA from primary tumours underwent library preparation using NEBNEXT Ultra II Directional RNA Library Prep Kit for Illumina and sequenced on an Illumina NovaSeq 6000 S2 platform acquiring paired end reads.

To evaluate the quality of paired-end RNA-sequencing data, FastQC and FastQ Screen [95] were run on fastq files and a summarised report was generated using MultiQC (v1.9)[96]. Reads were trimmed using Trim Galore (v0.6.6). Trimmed reads were aligned to the human reference genome GRCh38, using STAR 2.7.6a[97] with *--quantMode GeneCounts* and *--twopassMode Basic* alignment settings. Annotation file used for feature quantification was downloaded from GENCODE (v22) in GTF file format.

Cell lines

DU4475, MDA-MB-134-VI, T-47D and ZR-75-30, MCF7 $^{CDH1+/+}$ and MCF7 $^{CDH1-/-}$ cell lines[61] were Isacke laboratory stocks, were short tandem repeat tested (GenePrint 10 ID System; Promega) and tested routinely for mycoplasma (MycoAlert; Lonza) contamination. Cells were cultured in RPMI plus 10% FBS in 2D on tissue culture plates or in 3D in non-adherent suspension plates in a 1:1 mix of growth factor-reduced Matrigel (BD Biosciences) and RPMI plus 10% FBS. Cell lines used for RNASeq were cultured in 3D in non-adherent suspension plates in a 1:1 mix of growth factor-reduced Matrigel (BD Biosciences) and OcellO primary organoid media. Total RNA was extracted as above.

Generation of CSF-cell derived patient organoids

CSF collected in a sterile universal container was placed on ice for transport to laboratory. 96-well round-bottom suspension plate was warmed at 37°C at least 30 minutes prior, and Matrigel (growth factor reduced, Corning) was placed on ice. The sample was transferred to sterilised 2 mL V bottom tubes and centrifuged at 300*g* for 10 minutes. CSF supernatant was removed, and the remaining cell pellet was reconstituted in primary organoid media to 10 µL.

An equivalent volume of Matrigel was added and mixed by pipetting. 10 µL of sample mixture was pipetted per well of 96-well round bottom suspension culture plate, and placed in a tissue culture incubator 37°C for 30 minutes, prior to adding 150 µL media. Culture media was composed of 50% primary organoid media (OcellO), 50% meningeal cell conditioned primary organoid media, supplemented with neuregulin-1 10 ng/mL, EGF 10 ng/mL, and for ER+ breast cancers (from primary tumour histology), 17β-oestradiol (10^{-11} M). Culture media was changed every 7 days. All established organoids were regularly tested for mycoplasma, and identity confirmed by short tandem repeats (STR) testing using GenePrint 10 (Promega), with comparison to patient germline or primary tumour DNA. For lentiviral transductions, organoids were dissociated into single cells using TrypLE enzymes, resuspended in organoid media with the addition of lentiviral particles containing the PGK-H2BmCherry-IRES-Luc2 construct and polybrene (8 µg/mL). Cell/lentivirus mixtures were centrifuged at 800*g* at 32°C for 30 minutes, prior to culturing as suspension cells in low adherence 6-well plates for 48 hours. Cells were then collected and centrifuged to remove media containing virus and cultured in 50% Matrigel droplets. After 14 days cells were dissociated to single cells and FACS sorted using a FACSDiva (BD Biosciences) to select for mCherry-positive cells and returned to PDO culture.

In vitro PDO drug assays

Using Hamilton cold stage dissociated, BCLM PDO (3750 cells/well), MDA-MB-134-VI (3750 cells/well), T47-D (1500 cells/well), or DU4475 (1500 cells/well) were plated in 384-well clear flat bottom plates in 50% Matrigel:50% media droplets. 35 µL of organoid or cell line media were added to each well. 24 hours later, media containing methotrexate, crizotinib or taletrectinib in 0.2% DMSO or 0.2% DMSO alone (vehicle alone) was added to the wells and replenished on day 7. Cell viability was measured by CellTiter-Glo after 14 days.

Preparation of PDOs for histological analysis

Organoids growing in Matrigel droplets were prepared for histology by removing media and adding 4% paraformaldehyde solution to each well to cover droplets, and placed at room

temperature for 60 minutes. Organoids were then pipetted into a 15 mL Falcon tubes and washed twice with PBS. Organoids were collected at the bottom of the tube by gentle centrifugation (150*g* for 5 minutes) and resuspended in 50 - 100 µL of warmed HistoGel, and placed on Parafilm laid over ice for 5 minutes until solidified. HistoGel droplets containing organoids were then paraffin-embedded for sectioning and haematoxylin and eosin (H&E) and/or immunohistochemical staining **(Supplementary Table 7)**.

Establishment of patient-derived BCLM *in vivo* models

All animal work was carried out under UK Home Office Project Licenses 70/7413, P6AB1448A and PP4856884 granted under the Animals (Scientific Procedures) Act 1986 (Establishment Licence, X702B0E74 70/2902) and was approved by the "Animal Welfare and Ethical Review Body" at The Institute of Cancer Research (ICR). All mice were housed in individually ventilated cages, monitored daily by ICR Biological Services Unit staff and had food and water *ad libitum*. Mice were weighed at least two times per week. All experiment were performed with female 6-8 week NSG mice (Charles River). For PDOs KCL320, KCL450 and KCL566 sustained-release 17β-oestradiol pellets (0.36 mg/pellet, 90 day release, Innovative Research of America) were placed subcutaneously 7 days before tumour implantation.

Mammary fat pad inoculation*:* Mice were anaesthetized using isoflurane, and placed supine on a heat pad. Forceps were used to gently lift the 4th mammary fat pad nipple, and undissociated PDOs in 100 µL total (50% PBS: 50% growth factor-reduced Matrigel) were injected into the fat pad underlying nipple. Tumour growth was measured twice weekly up to a maximum diameter of 18 mm. Tumour volume was calculated using the following formula: Volume = 0.5236 x $[(\text{width} + \text{length})/2]^3$.

Intraductal inoculation

Intraductal inoculation was performed as previously described[98]. In brief, cells were inoculated bilaterally into the 3rd, 4th and 5th mammary glands (6 glands/mouse).

Intraperitoneal inoculation:

2 x 10^6 dissociated cells in 100 µL PBS were injected intraperitoneally without need for anaesthesia. Mice were monitored by weight (sudden increase in weight assessed for development of ascites) or loss of condition.

Intracardiac inoculation: Fur was removed from chest prior to procedure. Mice were anaesthetized with isoflurane and secured onto a VisualSonics Vevo-770 ultrasound imaging platform with continuous electrocardiogram monitoring. Ultrasound gel was applied over the chest. Organoids dissociated to single cells were passed through a 40 µm sieve. 5 x 10^5 cells in 100 µL sterile PBS were injected into the left ventricle under continuous ultrasound guidance. To confirm successful inoculation IVIS imaging was performed within 30 minutes of injection.

Intracerebroventricular (ICV) inoculation

Mice were anaesthetised with isoflurane, prior to depilation and midline incision of skin overlaying the skull and injected with 1×10^4 dissociated cells in 5 µL PBS into the right lateral cerebral ventricle at a rate of 2.5 µL tumour cells/min using a stereotaxic frame with pre-defined co-ordinates relative to bregma (x = 0.7 mm, y = + 0.6 mm, z = +2.0 mm). Following injection, the skin incision was closed.

Fixation, staining and imaging of tissues

Organs removed at necroscopy were fixed for 24 hours in 10% neutral buffered formalin at room temperature for 24 hours and paraffin-embedded for sectioning. For bone histology, soft tissue was stripped off prior to fixation in 10% neutral buffered formalin for 72 hours at 4°C, and decalcified in Hilleman and Lee EDTA solution (5.5% EDTA in 10% neutral buffered formalin) for 7 - 10 days. Once decalcification was complete, midline sagittal sections (whole head and spine) or coronal sections (whole head) were cut using a scalpel, and tissues were

paraffin-embedded for sectioning. Metastases were quantified from sections stained for human lamin A/C.

Statistics

All statistical tests were performed in GraphPad Prism 9 or R statistical environment (v3.6.0). Error bars indicate ± standard error of the mean (SEM). Significant differences were calculated by two-tailed un-paired Student's *t*-tests unless otherwise indicated. For multiple comparisons, a one-way analysis of variance (ANOVA) was used with Tukey's method of correction, and a confidence interval of 95%. One-way ANOVA with Dunnett's method of correction was used when multiple groups were compared to a single control group.

Data availability

The sequencing data generated by this work is derived from clinical samples. Raw data from have not been deposited due to ethical considerations. Requests for collaborative data sharing can be made to the corresponding author.

Graphical depictions were created with BioRender.com

References

1 Cagney, D. N. *et al.* Incidence and prognosis of patients with brain metastases at diagnosis of systemic malignancy: a population-based study. *Neuro Oncol* **19**, 1511-1521, doi:10.1093/neuonc/nox077 (2017).

2 Frisk, G. *et al.* Incidence and time trends of brain metastases admissions among breast cancer patients in Sweden. *Br J Cancer* **106**, 1850-1853, doi:10.1038/bjc.2012.163 (2012).

3 Leone, J. P. & Lin, N. U. Systemic Therapy of Central Nervous System Metastases of Breast Cancer. *Curr Oncol Rep* **21**, 49, doi:10.1007/s11912-019-0802-6 (2019).

4 Clarke, J. L., Perez, H. R., Jacks, L. M., Panageas, K. S. & Deangelis, L. M. Leptomeningeal metastases in the MRI era. *Neurology* **74**, 1449-1454, doi:10.1212/WNL.0b013e3181dc1a69 (2010).

5 Abouharb, S. *et al.* Leptomeningeal disease and breast cancer: the importance of tumor subtype. *Breast Cancer Res Treat* **146**, 477-486, doi:10.1007/s10549-014-3054-z (2014).

6 Morikawa, A. *et al.* Characteristics and Outcomes of Patients With Breast Cancer With Leptomeningeal Metastasis. *Clin Breast Cancer* **17**, 23-28, doi:10.1016/j.clbc.2016.07.002 (2017).

7 Kingston, B. *et al.* Treatment and prognosis of leptomeningeal disease secondary to metastatic breast cancer: A single-centre experience. *Breast* **36**, 54-59, doi:10.1016/j.breast.2017.07.015 (2017).

8 Niwinska, A., Rudnicka, H. & Murawska, M. Breast cancer leptomeningeal metastasis: propensity of breast cancer subtypes for leptomeninges and the analysis of factors influencing survival. *Med Oncol* **30**, 408, doi:10.1007/s12032-012-0408-4 (2013).

9 Lara-Medina, F. *et al.* Clinical features and prognostic factors in patients with carcinomatous meningitis secondary to breast cancer. *Breast J* **18**, 233-241, doi:10.1111/j.1524-4741.2012.01228.x (2012).

10 Lee, S. *et al.* Leptomeningeal metastases from breast cancer: intrinsic subtypes may affect unique clinical manifestations. *Breast Cancer Res Treat* **129**, 809-817, doi:10.1007/s10549-011-1682-0 (2011).

11 Clatot, F. *et al.* Clinical improvement and survival in breast cancer leptomeningeal metastasis correlate with the cytologic response to intrathecal chemotherapy. *J Neurooncol* **95**, 421-426, doi:10.1007/s11060-009-9940-2 (2009).

12 Le Rhun, E. *et al.* A retrospective case series of 103 consecutive patients with leptomeningeal metastasis and breast cancer. *J Neurooncol* **113**, 83-92, doi:10.1007/s11060-013-1092-8 (2013).

13 Makki, J. Diversity of Breast Carcinoma: Histological Subtypes and Clinical Relevance. *Clin Med Insights Pathol* **8**, 23-31, doi:10.4137/CPath.S31563 (2015).

14 Chen, Z. *et al.* Invasive lobular carcinoma of the breast: A special histological type compared with invasive ductal carcinoma. *PLoS One* **12**, e0182397, doi:10.1371/journal.pone.0182397 (2017).

15 McCart Reed, A. E., Kutasovic, J. R., Lakhani, S. R. & Simpson, P. T. Invasive lobular carcinoma of the breast: morphology, biomarkers and 'omics. *Breast Cancer Res* **17**, 12, doi:10.1186/s13058-015-0519-x (2015).

16 Tan, P. H. *et al.* The 2019 World Health Organization classification of tumours of the breast. *Histopathology* **77**, 181-185, doi:10.1111/his.14091 (2020).

17 Kingston, B. *et al.* Genomic profile of advanced breast cancer in circulating tumour DNA. *Nat Commun* **12**, 2423, doi:10.1038/s41467-021-22605-2 (2021).

18 Nguyen, B. *et al.* Genomic characterization of metastatic patterns from prospective clinical sequencing of 25,000 patients. *Cell* **185**, 563-575 e511, doi:10.1016/j.cell.2022.01.003 (2022).

19 Razavi, P. *et al.* The Genomic Landscape of Endocrine-Resistant Advanced Breast Cancers. *Cancer Cell* **34**, 427-438 e426, doi:10.1016/j.ccell.2018.08.008 (2018).

20 Robinson, D. R. *et al.* Integrative clinical genomics of metastatic cancer. *Nature* **548**, 297-303, doi:10.1038/nature23306 (2017).

21 Sivakumar, S. *et al.* Tissue and liquid biopsy profiling reveal convergent tumor evolution and therapy evasion in breast cancer. *Nat Commun* **13**, 7495, doi:10.1038/s41467-022-35245-x (2022).

22 Yates, L. R. *et al.* Genomic Evolution of Breast Cancer Metastasis and Relapse. *Cancer Cell* **32**, 169-184 e167, doi:10.1016/j.ccell.2017.07.005 (2017).

23 Zehir, A. *et al.* Mutational landscape of metastatic cancer revealed from prospective clinical sequencing of 10,000 patients. *Nat Med* **23**, 703-713, doi:10.1038/nm.4333 (2017).

24 Fitzpatrick, A. *et al.* Assessing CSF ctDNA to Improve Diagnostic Accuracy and Therapeutic Monitoring in Breast Cancer Leptomeningeal Metastasis. *Clin Cancer Res* **28**, 1180-1191, doi:10.1158/1078-0432.CCR-21-3017 (2022).

25 Mattos-Arruda, L. D. *et al.* Cerebrospinal fluid-derived circulating tumour DNA better represents the genomic alterations of brain tumours than plasma. *Nature communications* **6**, 8839, doi:10.1038/ncomms9839 PMID - 26554728 (2015).

26 Alexandrov, L. B. *et al.* Signatures of mutational processes in human cancer. *Nature* **500**, 415-421, doi:10.1038/nature12477 (2013).

27 Lockman, P. R. *et al.* Heterogeneous blood-tumor barrier permeability determines drug efficacy in experimental brain metastases of breast cancer. *Clin Cancer Res* **16**, 5664-5678, doi:10.1158/1078-0432.CCR-10-1564 (2010).

28 Angus, L. *et al.* The genomic landscape of metastatic breast cancer highlights changes in mutation and signature frequencies. *Nature Genetics* **51**, 1450-1458, doi:10.1038/s41588-019-0507-7 PMID - 31570896 (2019).

29 Curtis, C. *et al.* The genomic and transcriptomic architecture of 2,000 breast tumours reveals novel subgroups. *Nature* **486**, 346-352, doi:10.1038/nature10983 (2012).

30 Goh, J. Y. *et al.* Chromosome 1q21.3 amplification is a trackable biomarker and actionable target for breast cancer recurrence. *Nat Med* **23**, 1319-1330, doi:10.1038/nm.4405 (2017).

31 Brastianos, P. K. *et al.* Single-arm, open-label phase 2 trial of pembrolizumab in patients with leptomeningeal carcinomatosis. *Nature Medicine* **26**, 1280 - 1284 (2020).

32 Lefebvre, C. *et al.* Mutational Profile of Metastatic Breast Cancers: A Retrospective Analysis. *PLoS Med* **13**, e1002201, doi:10.1371/journal.pmed.1002201 (2016).

33 Ciriello, G. *et al.* Comprehensive Molecular Portraits of Invasive Lobular Breast Cancer. *Cell* **163**, 506-519, doi:10.1016/j.cell.2015.09.033 (2015).

34 Desmedt, C. *et al.* Genomic Characterization of Primary Invasive Lobular Breast Cancer. *J Clin Oncol* **34**, 1872-1881, doi:10.1200/JCO.2015.64.0334 (2016).

35 Drees, F., Pokutta, S., Yamada, S., Nelson, W. J. & Weis, W. I. Alpha-catenin is a molecular switch that binds E-cadherin-beta-catenin and regulates actin-filament assembly. *Cell* **123**, 903-915, doi:10.1016/j.cell.2005.09.021 (2005).

36 de Groot, J. S. *et al.* alphaE-catenin is a candidate tumor suppressor for the development of E-cadherin-expressing lobular-type breast cancer. *J Pathol* **245**, 456-467, doi:10.1002/path.5099 (2018).

37 Mohl, M., Winkler, S., Wieland, T. & Lutz, S. Gef10--the third member of a Rho-specific guanine nucleotide exchange factor subfamily with unusual protein architecture. *Naunyn Schmiedebergs Arch Pharmacol* **373**, 333-341, doi:10.1007/s00210-006-0083-0 (2006).

38 Kas, S. M. *et al.* Insertional mutagenesis identifies drivers of a novel oncogenic pathway in invasive lobular breast carcinoma. *Nat Genet* **49**, 1219-1230, doi:10.1038/ng.3905 (2017).

39 Bruner, H. C. & Derksen, P. W. B. Loss of E-Cadherin-Dependent Cell-Cell Adhesion and the Development and Progression of Cancer. *Cold Spring Harb Perspect Biol* **10**, doi:10.1101/cshperspect.a029330 (2018).

40 Schipper, K. *et al.* Rebalancing of actomyosin contractility enables mammary tumor formation upon loss of E-cadherin. *Nat Commun* **10**, 3800, doi:10.1038/s41467-019-11716-6 (2019).

41 Vasioukhin, V., Bauer, C., Degenstein, L., Wise, B. & Fuchs, E. Hyperproliferation and defects in epithelial polarity upon conditional ablation of alpha-catenin in skin. *Cell* **104**, 605-617, doi:10.1016/s0092-8674(01)00246-x (2001).

42 Lutchman, M. *et al.* Dematin interacts with the Ras-guanine nucleotide exchange factor Ras-GRF2 and modulates mitogen-activated protein kinase pathways. *Eur J Biochem* **269**, 638-649, doi:10.1046/j.0014-2956.2001.02694.x (2002).

43 Mohseni, M. & Chishti, A. H. The headpiece domain of dematin regulates cell shape, motility, and wound healing by modulating RhoA activation. *Mol Cell Biol* **28**, 4712-4718, doi:10.1128/MCB.00237-08 (2008).

44 Shen, H. *et al.* SCRIB Promotes Proliferation and Metastasis by Targeting Hippo/YAP Signalling in Colorectal Cancer. *Front Cell Dev Biol* **9**, 656359, doi:10.3389/fcell.2021.656359 (2021).

45 Nola, S. *et al.* Scrib regulates PAK activity during the cell migration process. *Hum Mol Genet* **17**, 3552-3565, doi:10.1093/hmg/ddn248 (2008).

46 Anastas, J. N. *et al.* A protein complex of SCRIB, NOS1AP and VANGL1 regulates cell polarity and migration, and is associated with breast cancer progression. *Oncogene* **31**, 3696-3708, doi:10.1038/onc.2011.528 (2012).

47 Ghosh, S. K., McCormick, T. S. & Weinberg, A. Human Beta Defensins and Cancer: Contradictions and Common Ground. *Front Oncol* **9**, 341, doi:10.3389/fonc.2019.00341 (2019).

48 Schackmann, R. C. *et al.* Cytosolic p120-catenin regulates growth of metastatic lobular carcinoma through Rock1-mediated anoikis resistance. *J Clin Invest* **121**, 3176-3188, doi:10.1172/JCI41695 (2011).

49 Sachs, N. *et al.* A Living Biobank of Breast Cancer Organoids Captures Disease Heterogeneity. *Cell* **172**, 373-386 e310, doi:10.1016/j.cell.2017.11.010 (2018).

50 Jung, J. *et al.* Discordances in ER, PR, and HER2 between primary breast cancer and brain metastasis. *J Neurooncol* **137**, 295-302, doi:10.1007/s11060-017-2717-0 (2018).

51 Li, B. D., Byskosh, A., Molteni, A. & Duda, R. B. Estrogen and progesterone receptor concordance between primary and recurrent breast cancer. *J Surg Oncol* **57**, 71-77, doi:10.1002/jso.2930570202 (1994).

52 Amir, E. *et al.* Prospective study evaluating the impact of tissue confirmation of metastatic disease in patients with breast cancer. *J Clin Oncol* **30**, 587-592, doi:10.1200/JCO.2010.33.5232 (2012).

53 Li, Z. *et al.* Mutual exclusivity of ESR1 and TP53 mutations in endocrine resistant metastatic breast cancer. *NPJ Breast Cancer* **8**, 62, doi:10.1038/s41523-022-00426-w (2022).

54 Thomson, A. H. *et al.* Changing molecular profile of brain metastases compared with matched breast primary cancers and impact on clinical outcomes. *Br J Cancer* **114**, 793-800, doi:10.1038/bjc.2016.34 (2016).

55 Priedigkeit, N. *et al.* Intrinsic Subtype Switching and Acquired ERBB2/HER2 Amplifications and Mutations in Breast Cancer Brain Metastases. *JAMA Oncol* **3**, 666-671, doi:10.1001/jamaoncol.2016.5630 (2017).

56 Duchnowska, R. *et al.* Conversion of epidermal growth factor receptor 2 and hormone receptor expression in breast cancer metastases to the brain. *Breast Cancer Res* **14**, R119, doi:10.1186/bcr3244 (2012).

57 Bartsch, R. *et al.* Trastuzumab deruxtecan in HER2-positive breast cancer with brain metastases: a single-arm, phase 2 trial. *Nat Med* **28**, 1840-1847, doi:10.1038/s41591-022-01935-8 (2022).

58 Perez-Garcia, J. M. *et al.* Trastuzumab Deruxtecan in Patients with Central Nervous System Involvement from HER2-Positive Breast Cancer: The DEBBRAH Trial. *Neuro Oncol*, doi:10.1093/neuonc/noac144 (2022).

59 Boire, A. *et al.* Complement Component 3 Adapts the Cerebrospinal Fluid for Leptomeningeal Metastasis. *Cell* **168**, 1101-1113 e1113, doi:10.1016/j.cell.2017.02.025 (2017).

60 Bumpers, H. L., Hassett, J. M., Jr., Penetrante, R. B., Hoover, E. L. & Holyoke, E. D. Endocrine organ metastases in subjects with lobular carcinoma of the breast. *Arch Surg* **128**, 1344-1347, doi:10.1001/archsurg.1993.01420240052009 (1993).

61 Bajrami, I. *et al.* E-Cadherin/ROS1 Inhibitor Synthetic Lethality in Breast Cancer. *Cancer Discov* **8**, 498-515, doi:10.1158/2159-8290.CD-17-0603 (2018).

62 Brastianos, P. K. *et al.* Genomic Characterization of Brain Metastases Reveals Branched Evolution and Potential Therapeutic Targets. *Cancer Discov* **5**, 1164-1177, doi:10.1158/2159-8290.CD-15-0369 (2015).

63 Malani, R. *et al.* Cerebrospinal fluid circulating tumor cells as a quantifiable measurement of leptomeningeal metastases in patients with HER2 positive cancer. *J Neurooncol* **148**, 599-606, doi:10.1007/s11060-020-03555-z (2020).

64 Christgen, M. & Derksen, P. Lobular breast cancer: molecular basis, mouse and cellular models. *Breast Cancer Res* **17**, 16, doi:10.1186/s13058-015-0517-z (2015).

65 Derksen, P. W. *et al.* Mammary-specific inactivation of E-cadherin and p53 impairs functional gland development and leads to pleomorphic invasive lobular carcinoma in mice. *Dis Model Mech* **4**, 347-358, doi:10.1242/dmm.006395 (2011).

66 Onder, T. T. *et al.* Loss of E-cadherin promotes metastasis via multiple downstream transcriptional pathways. *Cancer Res* **68**, 3645-3654, doi:10.1158/0008-5472.CAN-07-2938 (2008).

67 He, H., Gonzalez, A., Robinson, E. & Yang, W. T. Distant metastatic disease manifestations in infiltrating lobular carcinoma of the breast. *AJR Am J Roentgenol* **202**, 1140-1148, doi:10.2214/AJR.13.11156 (2014).

68 Joseph, J. *et al.* Rho guanine nucleotide exchange factor ARHGEF10 is a putative tumor suppressor in pancreatic ductal adenocarcinoma. *Oncogene* **39**, 308-321, doi:10.1038/s41388-019-0985-1 (2020).

69 Chi, Y. *et al.* Cancer cells deploy lipocalin-2 to collect limiting iron in leptomeningeal metastasis. *Science* **369**, 276-282, doi:10.1126/science.aaz2193 (2020).

70 Ratze, M. A. K. *et al.* Loss of E-cadherin leads to Id2-dependent inhibition of cell cycle progression in metastatic lobular breast cancer. *Oncogene* **41**, 2932-2944, doi:10.1038/s41388-022-02314-w (2022).

71 Boogerd, W. *et al.* The relevance of intraventricular chemotherapy for leptomeningeal metastasis in breast cancer: a randomised study. *Eur J Cancer* **40**, 2726-2733, doi:10.1016/j.ejca.2004.08.012 (2004).

72 Van Baelen, K. *et al.* Current and future diagnostic and treatment strategies for patients with invasive lobular breast cancer. *Ann Oncol* **33**, 769-785, doi:10.1016/j.annonc.2022.05.006 (2022).

73 Telford, B. J. *et al.* Synthetic Lethal Screens Identify Vulnerabilities in GPCR Signaling and Cytoskeletal Organization in E-Cadherin-Deficient Cells. *Mol Cancer Ther* **14**, 1213-1223, doi:10.1158/1535-7163.MCT-14-1092 (2015).

74 Kircher, M., Sawyer, S. & Meyer, M. Double indexing overcomes inaccuracies in multiplex sequencing on the Illumina platform. *Nucleic Acids Res* **40**, e3, doi:10.1093/nar/gkr771 (2012).

75 Van der Auwera, G. A. *et al.* From FastQ data to high confidence variant calls: the Genome Analysis Toolkit best practices pipeline. *Curr Protoc Bioinformatics* **43**, 11 10 11-11 10 33, doi:10.1002/0471250953.bi1110s43 (2013).

76 McKenna, A. *et al.* The Genome Analysis Toolkit: a MapReduce framework for analyzing next-generation DNA sequencing data. *Genome Res* **20**, 1297-1303, doi:10.1101/gr.107524.110 (2010).

77 Lee, S. *et al.* NGSCheckMate: software for validating sample identity in next-generation sequencing studies within and across data types. *Nucleic Acids Res* **45**, e103, doi:10.1093/nar/gkx193 (2017).

78 Cibulskis, K. *et al.* Sensitive detection of somatic point mutations in impure and heterogeneous cancer samples. *Nat Biotechnol* **31**, 213-219, doi:10.1038/nbt.2514 (2013).

79 Fan, Y. *et al.* MuSE: accounting for tumor heterogeneity using a sample-specific error model improves sensitivity and specificity in mutation calling from sequencing data. *Genome Biol* **17**, 178, doi:10.1186/s13059-016-1029-6 (2016).

80 Wilm, A. *et al.* LoFreq: a sequence-quality aware, ultra-sensitive variant caller for uncovering cell-population heterogeneity from high-throughput sequencing datasets. *Nucleic Acids Res* **40**, 11189-11201, doi:10.1093/nar/gks918 (2012).

81 Kim, S. *et al.* Strelka2: fast and accurate calling of germline and somatic variants. *Nat Methods* **15**, 591-594, doi:10.1038/s41592-018-0051-x (2018).

82 Wang, K., Li, M. & Hakonarson, H. ANNOVAR: functional annotation of genetic variants from high-throughput sequencing data. *Nucleic Acids Res* **38**, e164, doi:10.1093/nar/gkq603 (2010).

83 Adzhubei, I. A. *et al.* A method and server for predicting damaging missense mutations. *Nat Methods* **7**, 248-249, doi:10.1038/nmeth0410-248 (2010).

84 Kumar, P., Henikoff, S. & Ng, P. C. Predicting the effects of coding non-synonymous variants on protein function using the SIFT algorithm. *Nat Protoc* **4**, 1073-1081, doi:10.1038/nprot.2009.86 (2009).

85 Riester, M. *et al.* PureCN: copy number calling and SNV classification using targeted short read sequencing. *Source Code Biol Med* **11**, 13, doi:10.1186/s13029-016-0060-z (2016).

86 Blokzijl, F., Janssen, R., van Boxtel, R. & Cuppen, E. MutationalPatterns: comprehensive genome-wide analysis of mutational processes. *Genome Med* **10**, 33, doi:10.1186/s13073-018-0539-0 (2018).

87 Alexandrov, L. B. *et al.* The repertoire of mutational signatures in human cancer. *Nature* **578**, 94-101, doi:10.1038/s41586-020-1943-3 (2020).

88 Futreal, P. A. *et al.* A census of human cancer genes. *Nat Rev Cancer* **4**, 177-183, doi:10.1038/nrc1299 (2004).

89 Pereira, B. *et al.* The somatic mutation profiles of 2,433 breast cancers refines their genomic and transcriptomic landscapes. *Nat Commun* **7**, 11479, doi:10.1038/ncomms11479 (2016).

90 Nik-Zainal, S. *et al.* Landscape of somatic mutations in 560 breast cancer whole-genome sequences. *Nature* **534**, 47-54, doi:10.1038/nature17676 (2016).

91 Talevich, E., Shain, A. H., Botton, T. & Bastian, B. C. CNVkit: Genome-Wide Copy Number Detection and Visualization from Targeted DNA Sequencing. *PLoS Comput Biol* **12**, e1004873, doi:10.1371/journal.pcbi.1004873 (2016).

92 Van Loo, P. *et al.* Allele-specific copy number analysis of tumors. *Proc Natl Acad Sci U S A* **107**, 16910-16915, doi:10.1073/pnas.1009843107 (2010).

93 Roth, A. *et al.* PyClone: statistical inference of clonal population structure in cancer. *Nat Methods* **11**, 396-398, doi:10.1038/nmeth.2883 (2014).

94 Dang, H. X. *et al.* ClonEvol: clonal ordering and visualization in cancer sequencing. *Ann Oncol* **28**, 3076-3082, doi:10.1093/annonc/mdx517 (2017).

95 Wingett, S. W. & Andrews, S. FastQ Screen: A tool for multi-genome mapping and quality control. *F1000Res* **7**, 1338, doi:10.12688/f1000research.15931.2 (2018).

96 Ewels, P., Magnusson, M., Lundin, S. & Kaller, M. MultiQC: summarize analysis results for multiple tools and samples in a single report. *Bioinformatics* **32**, 3047-3048, doi:10.1093/bioinformatics/btw354 (2016).

97 Dobin, A. *et al.* STAR: ultrafast universal RNA-seq aligner. *Bioinformatics* **29**, 15-21, doi:10.1093/bioinformatics/bts635 (2013).

98 Sflomos, G. *et al.* A Preclinical Model for ERalpha-Positive Breast Cancer Points to the Epithelial Microenvironment as Determinant of Luminal Phenotype and Hormone Response. *Cancer Cell* **29**, 407-422, doi:10.1016/j.ccell.2016.02.002 (2016).

Table 1 | Clinicopathological characteristics of BCLM cohort

Study ID	Histological subtype	Time from pBC (years)	Time from mBC (years)	Parenchymal brain metastasis	Extracranial metastases	Extracranial disease status	Samples sequenced	BCLM survival (m)
KCL148	Lobular	4.7	4.7	None	Liver	Stable	CSF cfDNA, primary tumour	5.71
KCL320	Lobular	4.4	0.0	None	None	Absent	CSF cfDNA, primary tumour, PDO	5.50
KCL448	NST	4.3	1.0	Synchronous	Peritoneum, pericardium, distant nodes, soft tissue, bone	Progressive	CSF cfDNA, plasma cfDNA, primary tumour, skin metastasis	3.18
KCL449	Lobular	9.0	0.6	None	Bone	Stable	CSF cfDNA, primary tumour	27.43
KCL450	Lobular	14.0	1.0	None	Chest wall, peritoneal, pleura, bone	Progressive	CSF cfDNA, plasma cfDNA, primary tumour, PDO	1.39
KCL499	NST	0.7	0.0	Synchronous	None	Absent	CSF cfDNA, plasma cfDNA, primary tumour, second primary tumour	3.39
KCL523	Mixed	6.7	1.2	None	Peritoneum, bone, orbit	Stable	CSF cfDNA, plasma cfDNA, primary tumour	6.04
KCL553	Lobular	1.7	1.7	None	Peritoneum, pleura, ovaries, bone, orbit	Stable	CSF cfDNA, plasma cfDNA, primary tumour, ovary metastasis	18.39
KCL566	NST	6.7	1.1	Metachronous (stable)	Distant nodes, peritoneum, subcutaneous, bone	Progressive	CSF cfDNA, plasma cfDNA, primary tumour, nodal metastasis, PDO	0.86
KCL590	Micropapillary	2.6	2.6	None	Liver, spleen, bone	Progressive	CSF cfDNA, plasma cfDNA, primary tumour	1.29
KCL610	Lobular	6.5	6.5	None	Bone	Unknown	CSF cfDNA, plasma cfDNA, primary tumour	1.32
KCL616	Lobular	14.7	2.9	None	Bone, distant nodes	Unknown	CSF cfDNA, primary tumour	0.14
KCL617	Apocrine	1.0	0.0	None	Bone	Stable	CSF cfDNA, primary tumour	19.25
KCL622	Lobular	1.3	1.3	None	Bone, adrenal	Stable	CSF cfDNA, plasma cfDNA, primary tumour, PDO	3.64
KCL625	NST	11.1	0.0	None	None	Absent	CSF cfDNA, primary tumour, PDO	9.50
KCL650	NST	2.0	0.1	None	Liver, bone	Progressive	CSF cfDNA, plasma cfDNA	2.54
KCL658	NST	1.5	0.3	Metachronous (stable)	Skin	Progressive	CSF cfDNA, plasma cfDNA	9.75
KCL680	Lobular	0.7	0.7	None	Bone, peritoneum, ovaries	Stable	CSF cfDNA, primary tumour	25.61
RMH008	Lobular	4.3	2.0	Metachronous (stable)	Ovaries, cervix, vagina	Stable	CSF cfDNA, plasma cfDNA, ovary metastasis	0.93
RMH010	Lobular	10.6	4.0	Metachronous (stable)	Peritoneum, liver, bone, orbit	Progressive	CSF cfDNA, plasma cfDNA, primary tumour, liver metastasis	3.39
RMH011	NST	12.3	5.6	Metachronous (stable)	Lung, pleura, bone	Stable	CSF cfDNA, brain metastasis	18.64

BCLM, breast cancer leptomeningeal metastasis; cfDNA, cell-free DNA; CSF, cerebrospinal fluid; mBC, metastatic breast cancer; m, months; NST, no special type; PDO, patient-derived organoids; pBC, primary breast cancer. Metachronous, prior to BCLM diagnosis; Synchronous, diagnosed concurrenlty with BCLM.

Figure 1

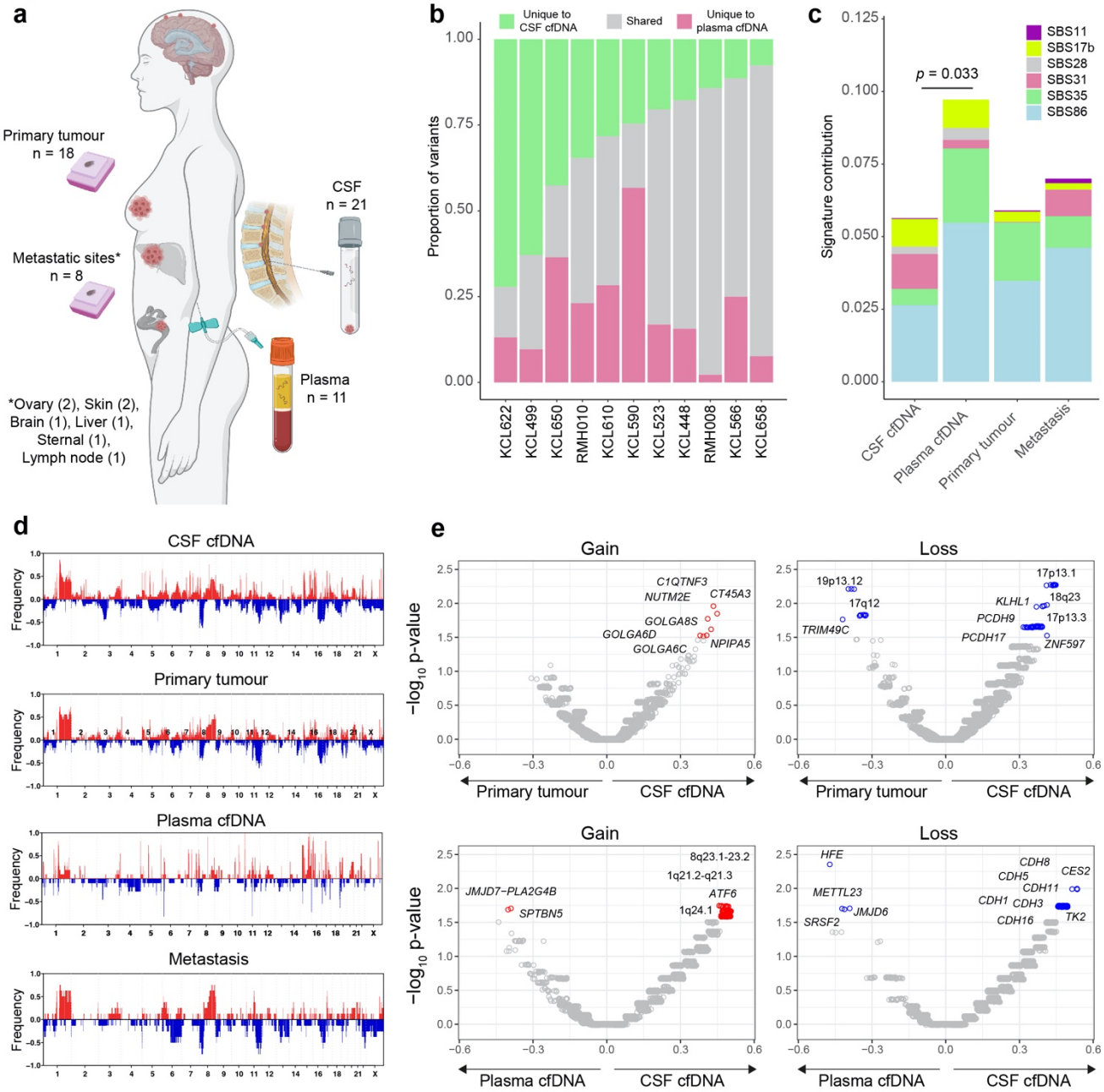
a
Primary tumour
n = 18
Metastatic sites*
n = 8
CSF
n = 21
Plasma
n = 11
*Ovary (2), Skin (2),
Brain (1), Liver (1),
Sternal (1),
Lymph node (1)
b
Unique to CSF cfDNA
Shared
Unique to plasma cfDNA
Proportion of variants
KCL622
KCL499
KCL650
RMH010
KCL610
KCL590
KCL523
KCL448
RMH008
KCL566
KCL658
c
SBS11
SBS17b
SBS28
SBS31
SBS35
SBS86
p = 0.033
Signature contribution
CSF cfDNA
Plasma cfDNA
Primary tumour
Metastasis
d
CSF cfDNA
Primary tumour
Plasma cfDNA
Metastasis
Frequency
e
Gain
Loss
C1QTNF3
NUTM2E
CT45A3
GOLGA8S
GOLGA6D
GOLGA6C
NPIPA5
19p13.12
17q12
TRIM49C
17p13.1
18q23
KLHL1
PCDH9
17p13.3
PCDH17
ZNF597
8q23.1-23.2
1q21.2-q21.3
ATF6
1q24.1
JMJD7-PLA2G4B
SPTBN5
HFE
METTL23
JMJD6
SRSF2
CDH8
CDH5
CES2
CDH11
CDH1
CDH3
CDH16
TK2
−log10 p-value
Primary tumour
CSF cfDNA
Plasma cfDNA

Fig. 1. Molecular profiling of BCLM by whole exome sequencing. **a** Schematic showing the sites of material collected. **b-e** Samples underwent WES and mutations (exonic variants excluding synonymous SNVs, plus splice variants) and copy number aberration (CNA) events identified. **b** WES of paired CSF cfDNA and plasma cfDNA sample collected at BCLM diagnosis, with sufficient (≥10%) cfDNA tumour content (*n* = 11 pairs). Bars show proportion of total variants shared or unique to either site. **c** Chemotherapy-related COSMIC Single Base Substitution (SBS) mutational signatures (chemo-SBS) compared between sites. Signature contributions of the six chemo-SBS were compared between CSF cfDNA, plasma cfDNA, primary and metastasis tumour samples. Stacked barplots display the mean signature contribution of each chemo-SBS, across all samples in each tissue category. Significantly different total chemo-SBS contribution is shown (Mann-Whitney test). **d** Genome wide purity-adjusted CNA plots of all samples (CSF cfDNA (*n* = 21), plasma cfDNA (*n* = 11), primary tumour (*n* = 18) and metastasis (*n* =8) showing frequency of copy number gain (red bars, positive y-axis) and copy number loss (blue bars, negative y-axis) at a gene level. **e** Volcano plots displaying differences in CNA per gene, between CSF cfDNA and primary tumours (upper panels) and between CSF cfDNA and plasma cfDNA (lower panels). Delta proportion (y-axis) is the proportional difference in CNA between tissues. Significance (x-axis, $-\log_{10}$ p-value) obtained by Chi-squared proportion tests, compares CNA proportion altered per gene between tissues. Gene names are annotated if delta proportion is ≥±0.20 and $-\log_{10}$ p-value ≥1.5.

Figure 2

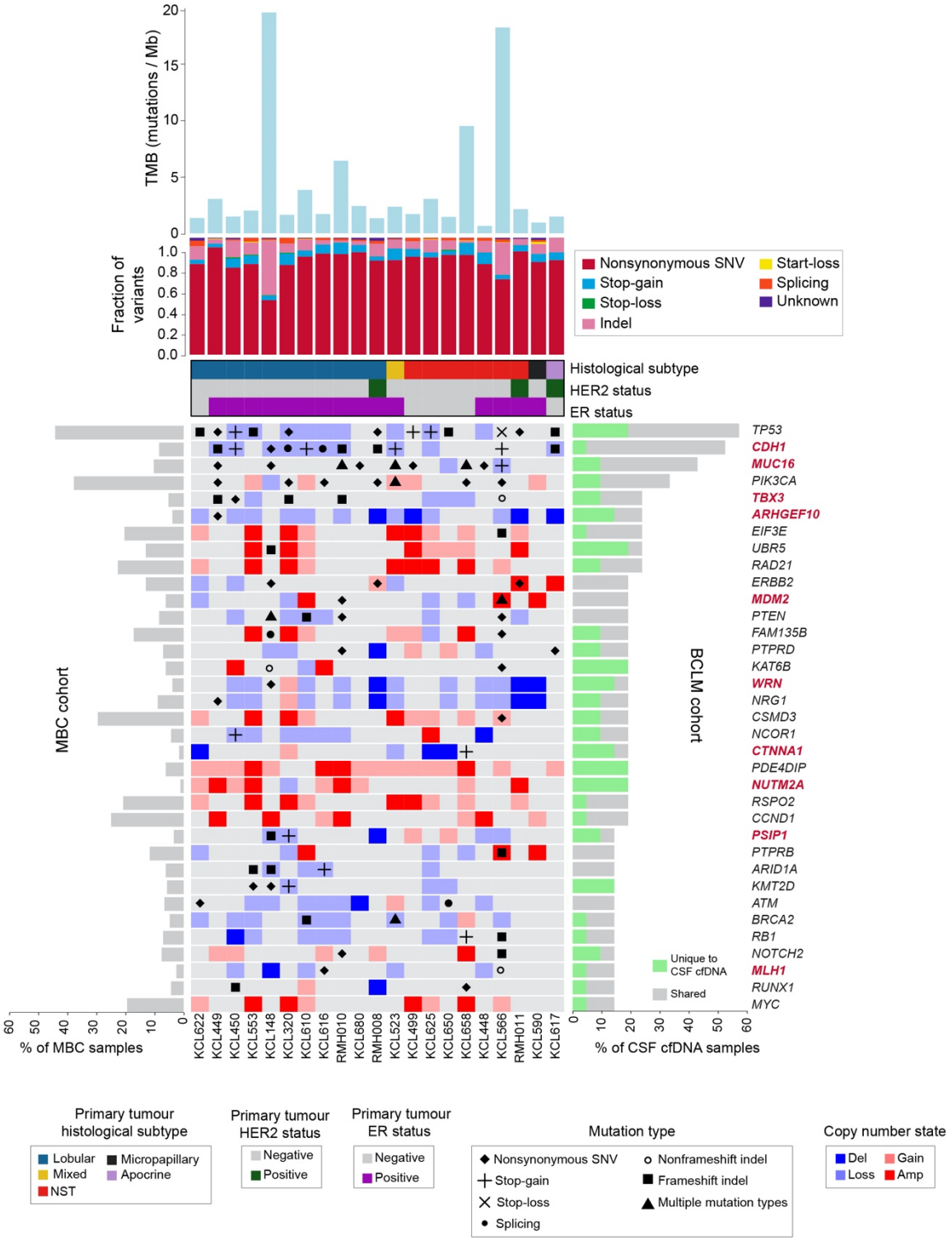
TMB (mutations / Mb)
Fraction of variants
Nonsynonymous SNV
Stop-gain
Stop-loss
Indel
Start-loss
Splicing
Unknown
Histological subtype
HER2 status
ER status
MBC cohort
BCLM cohort
TP53
CDH1
MUC16
PIK3CA
TBX3
ARHGEF10
EIF3E
UBR5
RAD21
ERBB2
MDM2
PTEN
FAM135B
PTPRD
KAT6B
WRN
NRG1
CSMD3
NCOR1
CTNNA1
PDE4DIP
NUTM2A
RSPO2
CCND1
PSIP1
PTPRB
ARID1A
KMT2D
ATM
BRCA2
RB1
NOTCH2
MLH1
RUNX1
MYC
Unique to CSF cfDNA
Shared
% of MBC samples
% of CSF cfDNA samples
KCL622
KCL449
KCL450
KCL553
KCL148
KCL320
KCL610
KCL616
RMH010
KCL680
RMH008
KCL523
KCL499
KCL625
KCL650
KCL658
KCL448
KCL566
RMH011
KCL590
KCL617
Primary tumour histological subtype
Lobular
Micropapillary
Mixed
Apocrine
NST
Primary tumour HER2 status
Negative
Positive
Primary tumour ER status
Negative
Positive
Mutation type
Nonsynonymous SNV
Nonframeshift indel
Stop-gain
Frameshift indel
Stop-loss
Multiple mutation types
Splicing
Copy number state
Del
Gain
Loss
Amp

Fig. 2 Cancer-associated mutation and copy number landscape of BCLM CSF cfDNA samples. Uppermost bar plot show tumour mutational burden (TMB) by sample. Stacked barplot below shows mutational subtype for each sample as fraction of all variants (excluding synonymous). Banners indicate primary tumour histological subtype and ER and HER2 status. Main plot shows the 36 most frequently cancer-associated altered genes (alterations include mutation and high-level copy number events) in CSF cfDNA as follows; Cancer Gene Census (CGC) gene altered in at least 4 cases; breast cancer driver gene (defined in Methods) altered in at least 3 cases. Gene names are highlighted in red if genetic alteration rate was significantly different ($p \leq 0.05$ by Chi-square test) to publicly-available dataset of 216 metastatic breast cancer (MBC) samples (see Methods). Right side bar plot shows percentage of CSF cfDNA samples ($n = 21$) with gene alterations that are unique to the CSF sample (green) or shared with any other site per individual (grey). Left side barplot shows total alteration rate in the MBC cohort. See **Supplementary Fig. 2** for extended data for the 21 BCLM cases, including matched plasma cfDNA, primary tumour and metastasis samples.

Figure 3

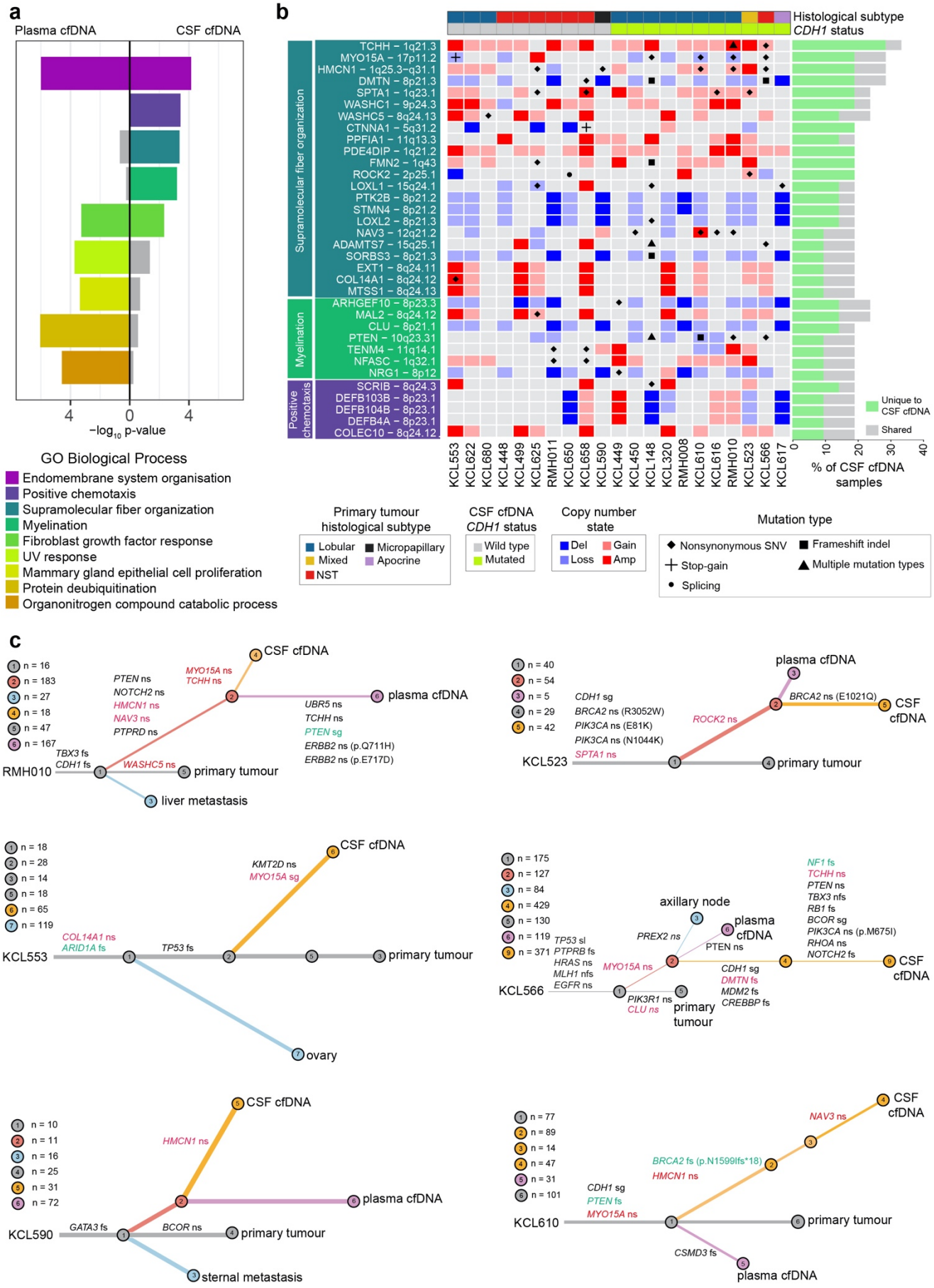
a
Plasma cfDNA
CSF cfDNA
4
0
4
−log10 p-value
GO Biological Process
Endomembrane system organisation
Positive chemotaxis
Supramolecular fiber organization
Myelination
Fibroblast growth factor response
UV response
Mammary gland epithelial cell proliferation
Protein deubiquitination
Organonitrogen compound catabolic process
b
Histological subtype
CDH1 status
Supramolecular fiber organization
Myelination
Positive chemotaxis
TCHH – 1q21.3
MYO15A – 17p11.2
HMCN1 – 1q25.3–q31.1
DMTN – 8p21.3
SPTA1 – 1q23.1
WASHC1 – 9p24.3
WASHC5 – 8q24.13
CTNNA1 – 5q31.2
PPFIA1 – 11q13.3
PDE4DIP – 1q21.2
FMN2 – 1q43
ROCK2 – 2p25.1
LOXL1 – 15q24.1
PTK2B – 8p21.2
STMN4 – 8p21.2
LOXL2 – 8p21.3
NAV3 – 12q21.2
ADAMTS7 – 15q25.1
SORBS3 – 8p21.3
EXT1 – 8q24.11
COL14A1 – 8q24.12
MTSS1 – 8q24.13
ARHGEF10 – 8p23.3
MAL2 – 8q24.12
CLU – 8p21.1
PTEN – 10q23.31
TENM4 – 11q14.1
NFASC – 1q32.1
NRG1 – 8p12
SCRIB – 8q24.3
DEFB103B – 8p23.1
DEFB104B – 8p23.1
DEFB4A – 8p23.1
COLEC10 – 8q24.12
KCL553
KCL622
KCL680
KCL448
KCL499
KCL625
RMH011
KCL650
KCL658
KCL590
KCL449
KCL450
KCL148
KCL320
RMH008
KCL610
KCL616
RMH010
KCL523
KCL566
KCL617
Unique to CSF cfDNA
Shared
0
10
20
30
40
% of CSF cfDNA samples
Primary tumour histological subtype
Lobular
Micropapillary
Mixed
Apocrine
NST
CSF cfDNA CDH1 status
Wild type
Mutated
Copy number state
Del
Gain
Loss
Amp
Mutation type
Nonsynonymous SNV
Frameshift indel
Stop-gain
Multiple mutation types
Splicing
c
n = 16
n = 183
n = 27
n = 18
n = 47
n = 167
RMH010
TBX3 fs
CDH1 fs
PTEN ns
NOTCH2 ns
HMCN1 ns
NAV3 ns
PTPRD ns
MYO15A ns
TCHH ns
WASHC5 ns
CSF cfDNA
plasma cfDNA
UBR5 ns
TCHH ns
PTEN sg
ERBB2 ns (p.Q711H)
ERBB2 ns (p.E717D)
primary tumour
liver metastasis
n = 40
n = 54
n = 5
n = 29
n = 42
KCL523
CDH1 sg
BRCA2 ns (R3052W)
PIK3CA ns (E81K)
PIK3CA ns (N1044K)
SPTA1 ns
ROCK2 ns
plasma cfDNA
BRCA2 ns (E1021Q)
CSF cfDNA
primary tumour
n = 18
n = 28
n = 14
n = 18
n = 65
n = 119
KCL553
COL14A1 ns
ARID1A fs
TP53 fs
KMT2D ns
MYO15A sg
CSF cfDNA
primary tumour
ovary
n = 175
n = 127
n = 84
n = 429
n = 130
n = 119
n = 371
KCL566
TP53 sl
PTPRB fs
HRAS ns
MLH1 nfs
EGFR ns
MYO15A ns
PREX2 ns
axillary node
plasma cfDNA
PTEN ns
PIK3R1 ns
CLU ns
primary tumour
CDH1 sg
DMTN fs
MDM2 fs
CREBBP fs
NF1 fs
TCHH ns
PTEN ns
TBX3 nfs
RB1 fs
BCOR sg
PIK3CA ns (p.M675I)
RHOA ns
NOTCH2 fs
CSF cfDNA
n = 10
n = 11
n = 16
n = 25
n = 31
n = 72
KCL590
GATA3 fs
HMCN1 ns
CSF cfDNA
plasma cfDNA
BCOR ns
primary tumour
sternal metastasis
n = 77
n = 89
n = 14
n = 47
n = 31
n = 101
KCL610
CDH1 sg
PTEN fs
MYO15A ns
BRCA2 fs (p.N1599lfs*18)
HMCN1 ns
NAV3 ns
CSF cfDNA
primary tumour
CSMD3 fs
plasma cfDNA

Fig. 3. BCLM enriched biological processes and subclone evolution. **a** Gene set enrichment analysis. Genes enriched for alterations (including mutation, amplification and deletion) in CSF cfDNA (*n* = 257) and/or plasma cfDNA (*n* = 160) *vs.* matched primary tumour, underwent statistical overrepresentation test using GO biological process (PANTHER). Displayed terms were retained if -$\log_{10}$ p-value (Fisher's exact test) was ≥3.0 in either sample type. **b** Focused alteration plot of genes from the indicated GO biological processes with -$\log_{10}$ p-value ≥3.0 in CSF cfDNA *vs*. matched tumour, but not in plasma cfDNA *vs*. primary tumour. Banners above indicate; histological subtype (primary tumour) and *CDH1* mutation status of CSF cfDNA. Left panel shows gene names and chromosomal location, grouped by GO biological processes. Bars to right show the frequency of gene alteration (including mutation, amplification and deletion) across CSF cfDNA samples (*n* = 21) with 'BCLM event' indicating alterations in CSF cfDNA or CSF cfDNA and plasma cfDNA at the time of BCLM diagnosis, and 'shared' being in both CSF cfDNA and archival tissue (primary tumour or metastasis sample). **c** Phylogenetic trees depicting BCLM clonal evolution. ClonEvol was used to infer consensus clonal evolution models, using the variant clusters and cellular prevalence generated by PyClone. Each branch represents the evolution path of a clone from its parental clone, and each node marks the clone number of the preceding branch. Samples are annotated at clone nodes when no further subclone evolution occurs. Branch lengths are scaled by the square root of number of mutations per clone, and branch width is inversely proportional to branch length. Mutations per clone number are shown to top left of the trees. Gene names and variant type are annotated on branches as follows; black font if appear in list of commonly altered cancer driver genes (**Fig. 2**) and/or breast cancer driver (defined in Methods); green font if variant is OncoKB annotated (**Supplementary Table 5**) as therapeutically actionable; red font are genes altered in CSF-enriched GO biological processes (see panels a and b above). Variant type abbreviations; ns, non-synonymous; sg, stop-gain; spl, splice-site variant; fs, frameshift.

Figure 4

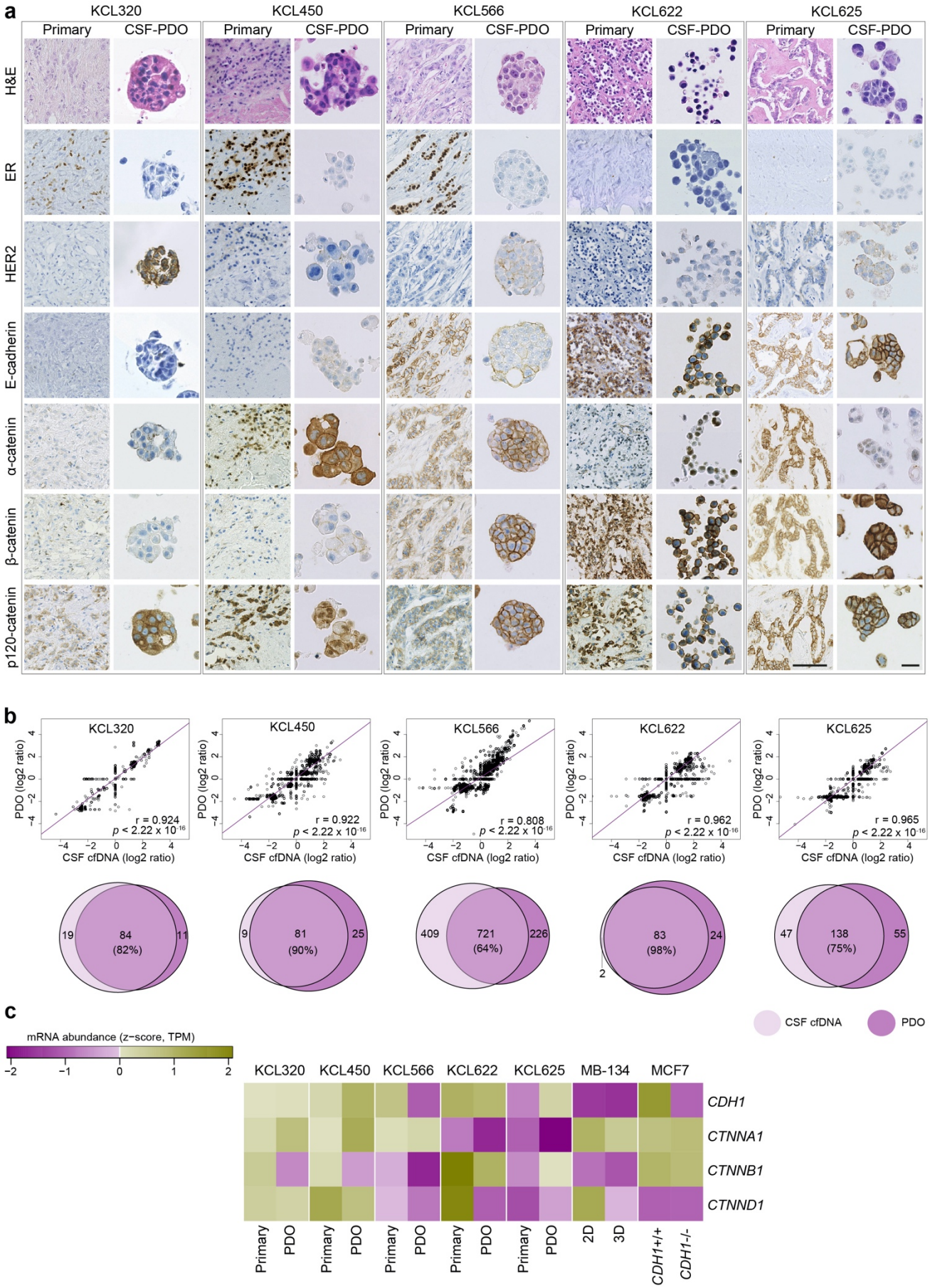
a
KCL320
KCL450
KCL566
KCL622
KCL625
Primary
CSF-PDO
H&E
ER
HER2
E-cadherin
α-catenin
β-catenin
p120-catenin
b
PDO (log2 ratio)
CSF cfDNA (log2 ratio)
r = 0.924
p < 2.22 x 10-16
r = 0.922
p < 2.22 x 10-16
r = 0.808
p < 2.22 x 10-16
r = 0.962
p < 2.22 x 10-16
r = 0.965
p < 2.22 x 10-16
19
84
(82%)
11
9
81
(90%)
25
409
721
(64%)
226
2
83
(98%)
24
47
138
(75%)
55
CSF cfDNA
PDO
c
mRNA abundance (z-score, TPM)
KCL320
KCL450
KCL566
KCL622
KCL625
MB-134
MCF7
CDH1
CTNNA1
CTNNB1
CTNND1
Primary
PDO
2D
3D
CDH1+/+
CDH1-/-

Fig. 4. Generation and characterisation of BCLM patient derived organoids (PDOs) established from CSF circulating tumour cells. **a** Histology and immunohistochemistry of BCLM PDOs and matched primary tumours. Scale bars, 50 µm. **b** Genetic comparison of CSF cfDNA and matched BCLM PDO (early passage) by WES. Top panel, correlation plots of copy number Z-score (one data point per gene) with regression line plotted (orange) and Pearson's r value plus significance shown. Lower panel, Venn diagrams of somatic mutations (excluding synonymous) present in CSF cfDNA and matched BCLM PDO, values shown are mutation count. **c** RNAseq of PDOs (fresh) and matched primary tumours (FFPE). Expression levels of adherens junction genes in PDOs and matched primary tumours. Values shown are Z-scores of log2-TPM values (transcripts per million) from RNASeq.

Figure 5

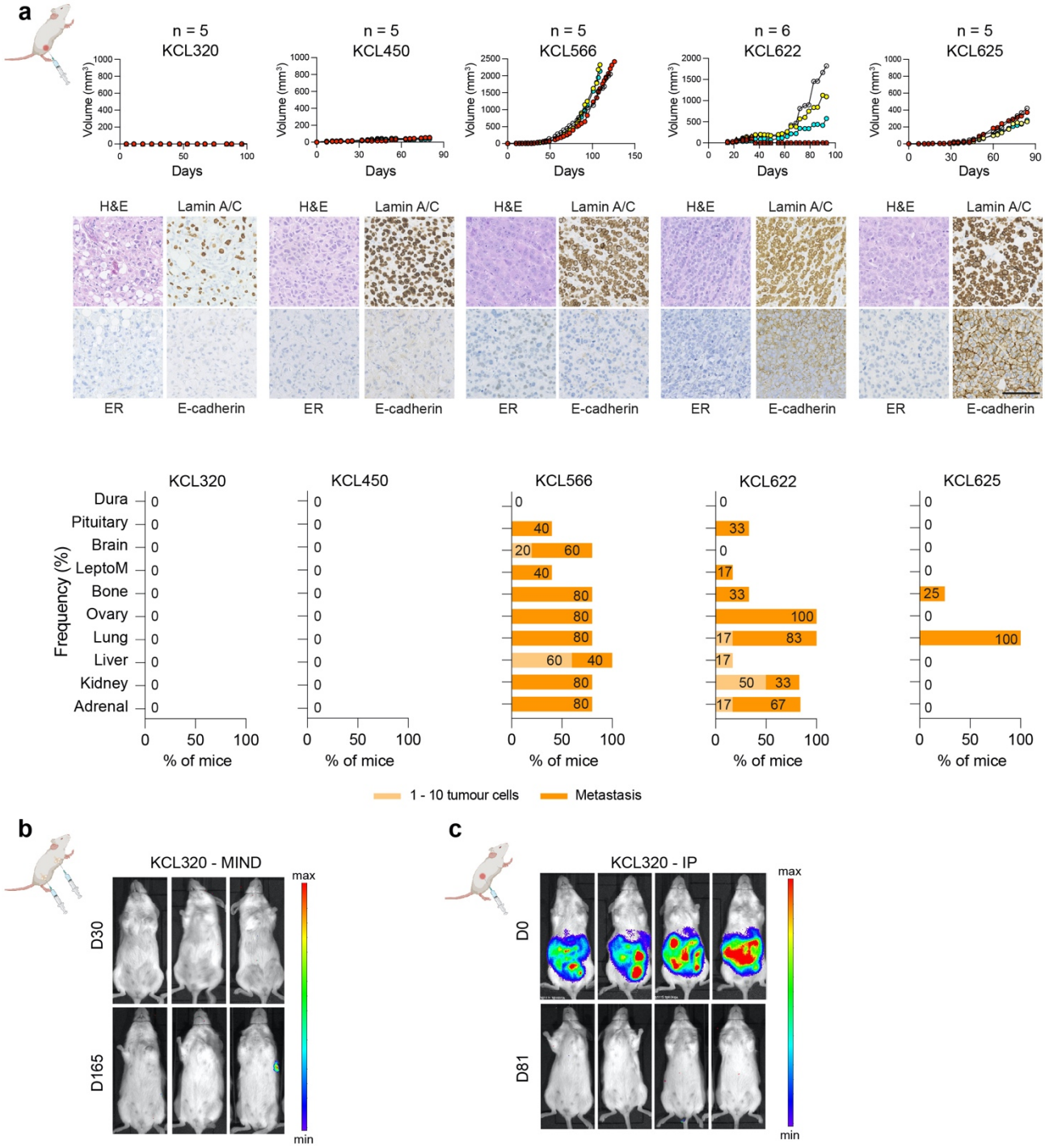
a
n = 5
KCL320
n = 5
KCL450
n = 5
KCL566
n = 6
KCL622
n = 5
KCL625
Volume (mm³)
Days
H&E
Lamin A/C
ER
E-cadherin
Frequency (%)
Dura
Pituitary
Brain
LeptoM
Bone
Ovary
Lung
Liver
Kidney
Adrenal
% of mice
1 - 10 tumour cells
Metastasis

b
KCL320 - MIND
D30
D165
max
min
c
KCL320 - IP
D0
D81
max
min

Fig. 5. Variable engraftment of BCLM PDOs in the orthotopic site. Female NSG mice were inoculated with mChLuc2-labelled PDOs as follows. **a** Non-dissociated BCLM PDOs (~1 x 10^6 cells) were injected transcutaneously into the 4th mammary fat pad (unilateral), *n* = 5 – 6 mice per PDO. Upper panel, tumour size was measured bi-weekly. Middle panel, mammary fat pad tumours stained for H&E, lamin A/C, ER and E-cadherin. Scale bar, 100 µm. Lower panel, bar charts show percentage of mice with metastatic dissemination in individual organs. Pale bars indicate % tissues with single or small cell clusters (1 - 10 cells), dark bars indicate tissues with metastatic deposits (>10 cells). **b** 4 x 10^4 dissociated cells per gland were inoculated via the mammary gland intraductal (MIND) route into the 3rd, 4th and 5th mammary glands, bilaterally (6 glands/mouse; *n* = 6 mice). Mice were IVIS imaged on day 0 and day 165 (endpoint). **c** 2 x 10^6 dissociated cells injected intraperitoneally (*n* = 4) with IVIS imaging at day 0 and day 81 (endpoint).

Figure 6

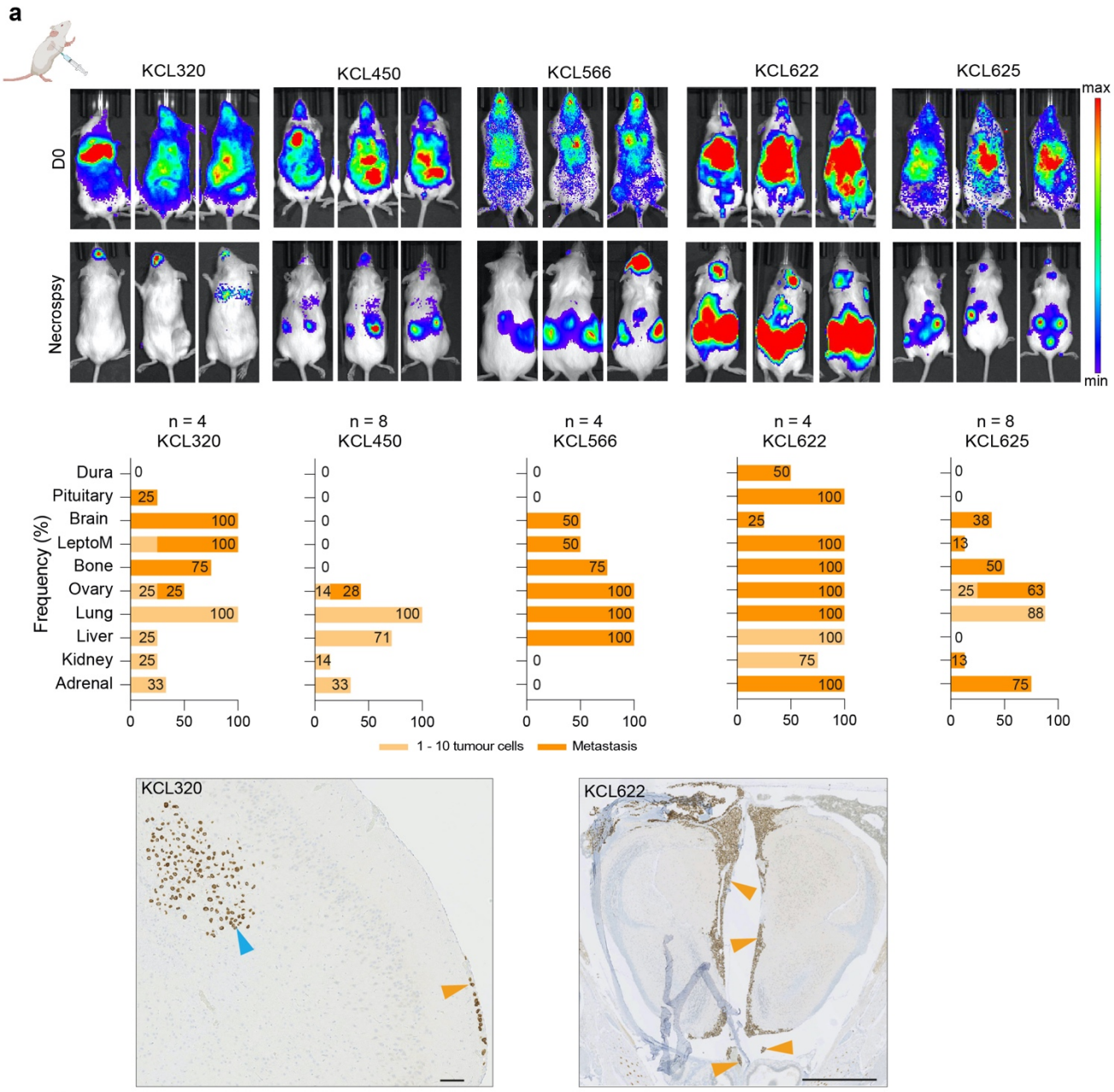
a
KCL320
KCL450
KCL566
KCL622
KCL625
D0
Necrospsy
max
min
n = 4
KCL320
n = 8
KCL450
n = 4
KCL566
n = 4
KCL622
n = 8
KCL625
Frequency (%)
Dura
Pituitary
Brain
LeptoM
Bone
Ovary
Lung
Liver
Kidney
Adrenal
1 - 10 tumour cells
Metastasis
KCL320
KCL622

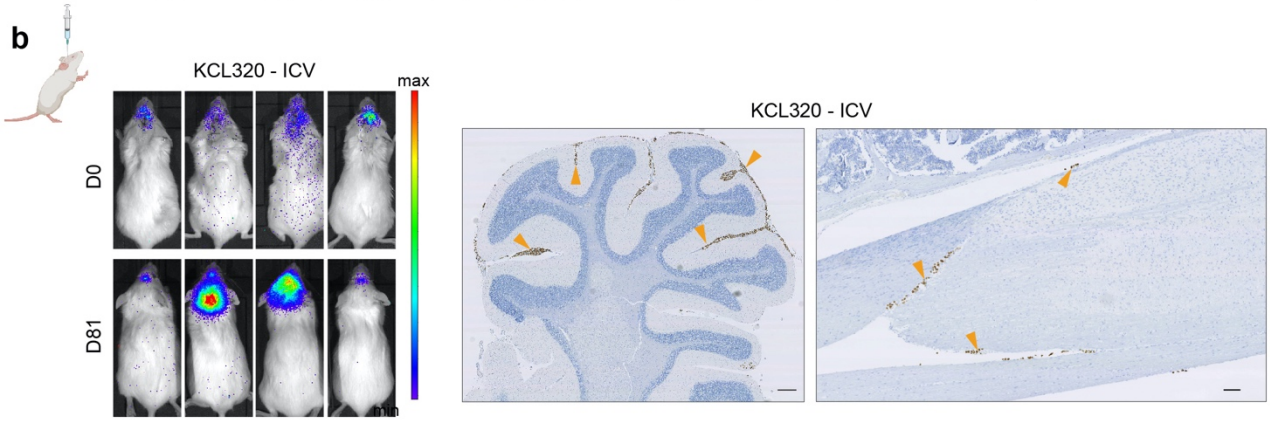
b
KCL320 - ICV
max
min
D0
D81
KCL320 - ICV

Fig. 6 Patient-derived xenograft models of BCLM. BCLM-PDOs were dissociated into single cells. **a** 0.5 - 1.0 x 10^6 cells inoculated into the left cardiac ventricle under ultrasound guidance. Upper panel, IVIS imaging immediately after cell injection (day 0) and at endpoint for each mouse (upon development of significant morbidity) day 40 - 210. Middle panel, metastatic site involvement assessed by lamin A/C staining of FFPE sections. Bar charts show percentage of mice with disseminated tumour cells in individual organs, with pale bars indicating with single or small clusters of cells (1 - 10 cells) and dark bars indicating tissues with metastatic deposits (>10 cells). Bottom panel. IHC staining for human lamin A/C of whole cranium and spine FFPE sections showing tumour cells growing along the meninges (orange arrowheads) or in the brain parenchyma (blue arrowheads). Scale bars; Left, 100 μm; Right, 1 mm. **b** 1 x 10^5 cells inoculated intracerebroventricularly (ICV) (n = 4 mice) with IVIS imaging on day 0 and day 81 (endpoint). Right panels show histology of cranium and spine FFPE sections stained for human lamin A/C. Orange arrowheads indicate leptomeningeal involvement. Scale bars; 250 μm.

Figure 7

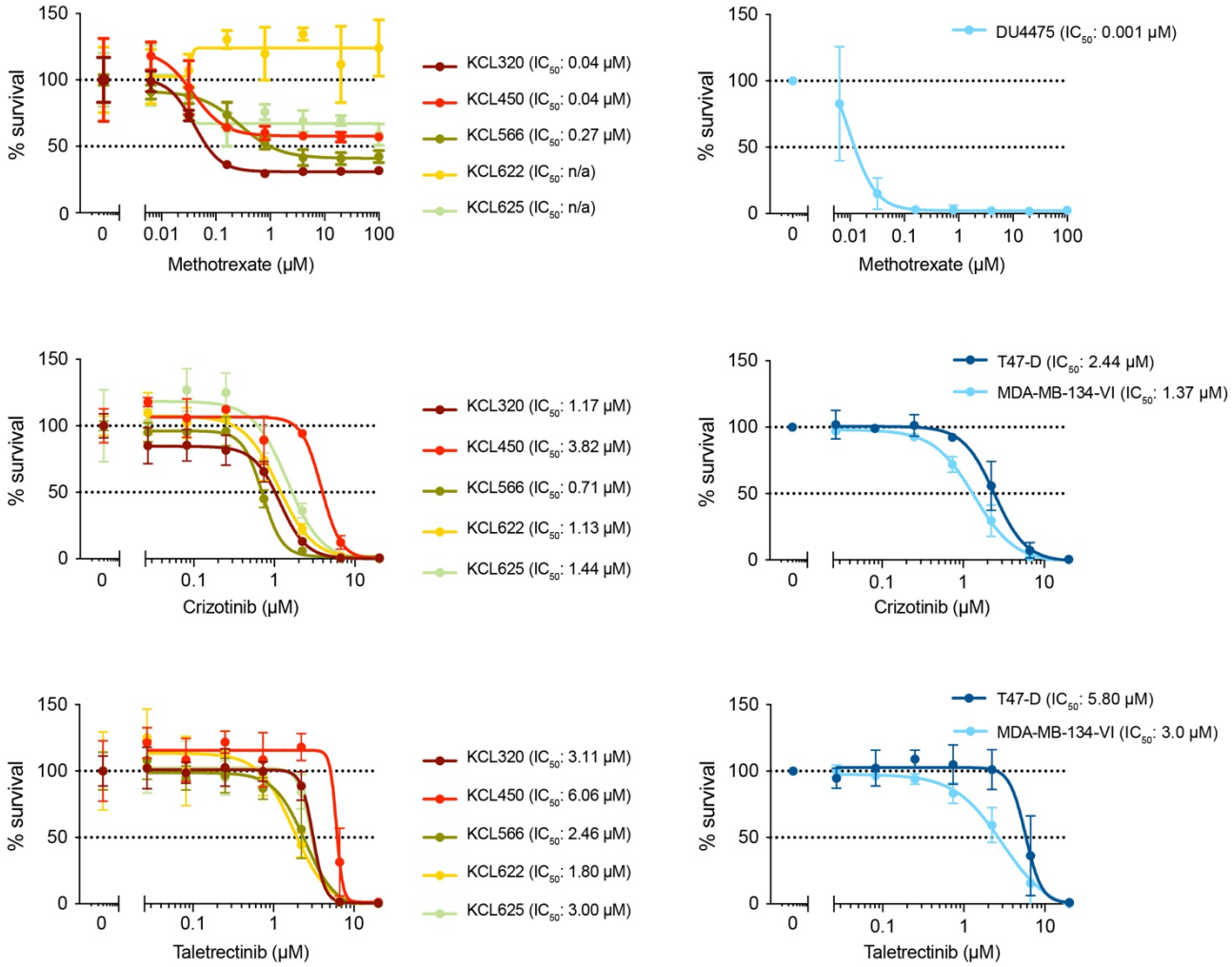

Fig. 7. Therapeutic targeting of BCLM PDOs. BCLM PDO and cell line controls were cultured in organoid conditions in the presence of methotrexate, crizotinib or taletrectinib in 0.2% DMSO or 0.2% DMSO alone (vehicle alone). Cell viability was measured by CellTiter-Glo after 14 days. Data represents mean of *n* = 4 wells per datapoint ±SD, normalised to vehicle alone treatment.

Genomic profiling and pre-clinical modelling of breast cancer leptomeningeal metastasis (BCLM) reveals acquisition of a lobular-like phenotype

Amanda Fitzpatrick, Marjan Iravani, Adam Mills, David Vicente, Thanussuyah Alaguthurai, Ioannis Roxanis, Nicholas C. Turner, Syed Haider, Andrew N.J. Tutt and Clare M. Isacke

Supplementary Material

Supplementary Table 1 | Patient cohort clinicopathological characteristics

Supplementary Table 2 | Whole exome sequencing and variant calling metrics

Supplementary Table 3 | COSMIC SBS mutational signatures across sample types

Supplementary Table 4 | Genetic alterations in BCLM *vs*. MBC cohort (uploaded as a separate file)

Supplementary Table 5 | OncoKB actionable gene alterations in CSF cfDNA

Supplementary Table 6 | Immunohistochemical scoring of primary tumours and matched BCLM PDOs

Supplementary Table 7 | Antibodies used for immunohistochemistry

Supplementary Figure 1 | Sequencing pipeline and metrics

Supplementary Figure 2 | Cancer-associated mutation and copy number landscape of all matched samples.

Supplementary Figure 3 | BCLM enriched biological processes.

Supplementary Figure 4 | BCLM subclone evolution.

Supplementary Figure 5 | Tagging BCLM patient-derived organoids.

Supplementary Table 1 | Patient cohort clinicopathological characteristics

	Patients (*n* = 21)	
	n	%
Age (years)		
Median	52	
Range	28 - 73	
Histological subtype		
Lobular	11	52.39
Mixed lobular/NST	1	4.76
NST	7	33.33
Micropapillary	1	4.76
Apocrine	1	4.76
Receptor subtype (primary tumour)		
ER+ HER2-	13	61.90
ER+ HER2+	2	9.52
ER- HER2+	1	4.76
TN	5	23.81
Staging at diagnosis		
N0	5	23.81
N1+	9	42.86
unknown N	1	4.76
M1	6	28.57
Chemotherapy (adjuvant/neoadjuvant)		
Yes	14	66.67
No	1	4.76
N/A (M1)	6	28.57
Endocrine therapy (adjuvant/neoadjuvant)		
Tamoxifen	3	20.00
Tamoxifen then AI	3	20.00
AI	4	26.67
N/A (M1)	5	33.33
Other metastatic sites		
None (BCLM only)	3	14.29
Brain parenchyma	7	33.33
Synchronous	2	9.52
Metachronous	5	23.81
Bone	15	71.43
Serosal	7	33.33
Soft tissue	7	33.33
Liver	4	19.05
Ovary	3	14.29
Nodal	3	14.29
Adrenal	1	4.76
Lung	1	4.76

AI, aromatase inhibitor; BCLM,breast cancer leptomeningeal metastasis; ER, oestrogen receptor; HER2, human epidermal growth factor receptor 2; M1, metastatic stage 1; N, nodal status; N/A, not applicable; TN, triple negative.

Supplementary Table 2 | Whole exome sequencing and variant calling metrics

	Mean coverage (Picard)		Somatic variants (total)		SNV (total)		Indel (total)	
	Median	*IQR*	*Median*	*Range*	*Median*	*Range*	*Median*	*Range*
CSF	165	104.8 - 211	125	40 - 1196	108	35 - 777	9	4 - 560
Plasma	317	283.7 - 362.3	124	34 - 464	113	29 - 371	7	3 - 116
Primary tumour	196	131.9 - 236.4	80	43 - 700	73	39 - 358	7	1 - 327
Recurrence	211	178.3 - 233.9	76	46 - 418	66	42 - 259	5	3 - 139
Germline	106	100.1 - 117.8	-	-	-	-	-	-

CSF, cerebrospinal fluid; IQR,interquartile range; SNV,single nucleotide variation.

Supplementary Table 3 | COSMIC SBS mutational signatures across sample types

	mean signature contributions				significance			
Signature	**CSF cfDNA**	**Plasma cfDNA**	**Primary tumour**	**Metastasis**	***p* value (CSF cfDNA vs. plasma cfDNA)**	***p* value (CSF cfDNA vs. metastasis)**	***p* value (CSF cfDNA vs. primary tumour)**	***p* value (plasma cfDNA vs. primary tumour)**
SBS1	0.0641	0.0785	0.1521	0.1193	0.6709	0.1316	**0.0105**	0.1278
SBS2	0.0401	0.0285	0.0169	0.0339	0.6252	0.8182	0.2262	0.4568
SBS3	0.0126	0.0297	0.0009	0.0143	0.3662	0.9103	0.2258	0.0863
SBS4	0.0065	0.0069	0.0091	0.0000	0.9609	0.4068	0.7394	0.8227
SBS5	0.0000	0.0000	0.0000	0.0065	-	0.1062	-	-
SBS6	0.0453	0.0252	0.0207	0.0207	0.4463	0.3359	0.1841	0.8502
SBS7a	0.0489	0.0345	0.0233	0.0552	0.4688	0.7892	0.1937	0.6226
SBS7b	0.0047	0.0019	0.0254	0.0079	0.4751	0.5606	0.1163	0.1891
SBS7c	0.0015	0.0006	0.0033	0.0000	0.6056	0.4347	0.4637	0.3863
SBS7d	0.0037	0.0001	0.0107	0.0063	0.2127	0.5328	0.1344	0.0670
SBS8	0.0125	0.0246	0.0038	0.0046	0.4189	0.4495	0.2622	0.1598
SBS10a	0.0019	0.0039	0.0076	0.0006	0.4335	0.4770	0.2100	0.5645
SBS10b	0.0462	0.0329	0.0904	0.0417	0.5491	0.8587	0.1282	0.1009
SBS10d	0.0000	0.0024	0.0000	0.0000	0.1708	-	-	0.2201
SBS11	0.0002	0.0000	0.0004	0.0016	0.4783	0.2056	0.7139	0.4315
SBS12	0.0000	0.0000	0.0001	0.0070	-	0.1062	0.2722	0.4315
SBS13	0.0870	0.1109	0.0265	0.0511	0.6102	0.4281	**0.0488**	**0.0217**
SBS14	0.0033	0.0078	0.0081	0.0045	0.3468	0.7758	0.2268	0.9584
SBS15	0.0642	0.0192	0.0605	0.0283	0.1575	0.3423	0.9203	0.2837
SBS16	0.0040	0.0098	0.0057	0.0161	0.3175	0.0886	0.7566	0.6238
SBS17a	0.0084	0.0040	0.0050	0.0062	0.4173	0.7089	0.4206	0.8015
SBS17b	0.0096	0.0098	0.0036	0.0022	0.9798	0.2727	0.2122	0.3204
SBS18	0.0354	0.0051	0.0049	0.0152	0.3240	0.5842	0.2191	0.9767
SBS19	0.0010	0.0013	0.0017	0.0032	0.8075	0.3064	0.6639	0.8566
SBS20	0.0074	0.0217	0.0098	0.0103	0.1814	0.6886	0.6552	0.3028
SBS21	0.0122	0.0134	0.0149	0.0416	0.9238	0.1184	0.7931	0.9112
SBS22	0.0057	0.0123	0.0091	0.0077	0.4331	0.8086	0.5518	0.6833
SBS23	0.0000	0.0016	0.0040	0.0041	0.1708	0.1062	**0.0353**	0.4071
SBS24	0.0292	0.0084	0.0390	0.0230	0.1294	0.7266	0.5861	0.1476
SBS26	0.0008	0.0099	0.0000	0.0021	0.1811	0.5008	0.3755	0.1860
SBS27	0.0001	0.0000	0.0003	0.0000	0.4783	0.5468	0.3387	0.2721
SBS28	0.0025	0.0041	0.0000	0.0000	0.6668	0.2976	0.1271	0.2201
SBS29	0.0027	0.0041	0.0128	0.0000	0.7371	0.5468	0.2354	0.4440
SBS30	0.0069	0.0168	0.0041	0.0160	0.3184	0.2774	0.5996	0.1708
SBS31	0.0120	0.0030	0.0002	0.0092	0.2944	0.7892	0.0808	0.2563
SBS32	0.0012	0.0018	0.0114	0.0023	0.7927	0.6387	0.1256	0.2939
SBS33	0.0027	0.0042	0.0023	0.0017	0.5898	0.6445	0.8493	0.5569
SBS34	0.0011	0.0012	0.0008	0.0010	0.9215	0.9218	0.7284	0.7006
SBS35	0.0056	0.0257	0.0201	0.0109	**0.0167**	0.4531	0.1112	0.6835
SBS36	0.0033	0.0074	0.0039	0.0002	0.5391	0.5072	0.8883	0.6230
SBS37	0.0092	0.0068	0.0137	0.0116	0.7517	0.7909	0.5815	0.4987
SBS38	0.0023	0.0038	0.0000	0.0029	0.7261	0.8748	0.3755	0.2201
SBS39	0.1124	0.1232	0.0715	0.0597	0.8260	0.2695	0.3106	0.3186
SBS42	0.0195	0.0077	0.0072	0.0313	0.4198	0.5455	0.3419	0.9558
SBS43	0.0065	0.0035	0.0053	0.0000	0.5661	0.2653	0.7971	0.6440
SBS44	0.0001	0.0000	0.0000	0.0030	0.4783	0.1247	0.3755	-
SBS45	0.0047	0.0125	0.0034	0.0000	0.3710	0.4773	0.7964	0.2647
SBS46	0.0064	0.0090	0.0108	0.0063	0.5935	0.9786	0.6092	0.8780
SBS48	0.0010	0.0012	0.0018	0.0005	0.8227	0.6294	0.4309	0.7182
SBS49	0.0044	0.0072	0.0014	0.0016	0.4929	0.4290	0.2195	0.1036
SBS50	0.0127	0.0185	0.0179	0.0000	0.5830	0.1682	0.6520	0.9739
SBS51	0.0016	0.0036	0.0001	0.0003	0.4047	0.4899	0.2455	0.1104
SBS52	0.0040	0.0061	0.0018	0.0000	0.6968	0.3851	0.5412	0.3789
SBS53	0.0017	0.0081	0.0054	0.0039	0.1177	0.3409	0.4450	0.7180
SBS54	0.0260	0.0156	0.0210	0.0248	0.3971	0.9345	0.6473	0.6235
SBS55	0.0790	0.0409	0.0665	0.1383	0.1853	0.1996	0.7074	0.4794
SBS57	0.0000	0.0003	0.0000	0.0000	0.1708	-	-	0.2201
SBS58	0.0000	0.0000	0.0025	0.0000	-	-	0.1145	0.2571
SBS59	0.0125	0.0051	0.0125	0.0075	0.2449	0.5020	0.9989	0.2311
SBS60	0.0037	0.0000	0.0010	0.0011	0.1620	0.4125	0.2480	0.4315
SBS84	0.0004	0.0018	0.0076	0.0263	0.3290	**0.0011**	0.1646	0.4269
SBS85	0.0000	0.0011	0.0000	0.0002	0.1708	0.1062	-	0.2201
SBS86	0.0264	0.0547	0.0347	0.0461	0.1464	0.3660	0.5532	0.3724
SBS87	0.0582	0.0715	0.0719	0.0516	0.5954	0.8302	0.4933	0.9898
SBS88	0.0071	0.0067	0.0054	0.0003	0.9597	0.3815	0.7734	0.8276
SBS89	0.0018	0.0062	0.0000	0.0000	0.3989	0.5468	0.3755	0.2201
SBS90	0.0000	0.0000	0.0000	0.0000	-	-	-	-
SBS91	0.0021	0.0109	0.0022	0.0064	0.1542	0.3520	0.9560	0.2139
SBS92	0.0000	0.0000	0.0035	0.0000	-	-	0.2722	0.4315
SBS93	0.0004	0.0007	0.0033	0.0000	0.7502	0.5468	0.3465	0.5366
SBS94	0.0016	0.0001	0.0142	0.0000	0.5204	0.5468	0.3324	0.4362

Significant *p* values highlighted in red

Supplementary Table 5 | OncoKB actionable gene alterations in CSF cfDNA

Patient ID	Gene	Alteration type	Alteration detail	Therapeutic level	Drug	Shared with primary tumour
KCL148	*BRCA1*	Frameshift insertion	p.Y655Vfs*18	1	Olaparib	not shared
KCL566	N/A	High tumour mutational burden	TMB >10 muts/Mb	1	Pembrolizumab	not shared
KCL566	*NF1*	Frameshift deletion	p.Y1586Ifs*17	4	Trametinib; Cobimetinib	not shared
KCL610	*BRCA2*	Frameshift deletion	p.N1599Ifs*18	1	Olaparib	not shared
KCL680	*ESR1*	Nonsynonymous SNV	p.Y537S	3A	Fulvestrant	not shared
KCL148	N/A	High tumour mutational burden	TMB >10 muts/Mb	1	Pembrolizumab	shared
KCL148	*ARID1A*	Frameshift deletion	p.P1468Lfs*13	4	Tazemetostat	shared
KCL148	*PTEN*	Frameshift insertion	p.E157Gfs*23	4	GSK2636771	shared
KCL148	*PTEN*	Frameshift insertion	p.G251Vfs*6	4	GSK2636771	shared
KCL148	*PTCH1*	Frameshift insertion	p.R1242Qfs*17	3B	Sonidegib,Vismodegib	shared
KCL320	*PIK3CA*	Nonsynonymous SNV	p.E542K	1	Alpelisib	shared
KCL448	*CDKN2A*	Stopgain	p.R80X	4	Abemaciclib	shared
KCL449	*PIK3CA*	Nonsynonymous SNV	p.H1047R	1	Alpelisib	shared
KCL450	*AKT1*	Nonsynonymous SNV	p.E17K	3	Capivasertib	shared
KCL523	*BRCA2*	Nonsynonymous SNV	p.R3052W	1	Olaparib	shared
KCL523	*PIK3CA*	Nonsynonymous SNV	p.N1044K	1	Alpelisib	shared
KCL553	*ARID1A*	Frameshift deletion	p.Q548Hfs*65	4	Tazemetostat	shared
KCL566	*MDM2*	Amplification	Amplification	4	Milademetan	shared
KCL590	*MDM2*	Amplification	Amplification	4	Milademetan	shared
KCL610	*PTEN*	Frameshift deletion	p.F21Yfs*16	4	GSK2636771	shared
KCL610	*MDM2*	Amplification	Amplification	4	Milademetan	shared
KCL616	*PIK3CA*	Nonsynonymous SNV	p.H1047R	1	Alpelisib	shared
KCL616	*ARID1A*	Stopgain	p.Q920X	4	Tazemetostat	shared
KCL617	*ERBB2*	Amplification	Amplification	1	Trastuzumab	shared
KCL622	*ATM*	Nonsynonymous SNV	p.R337H	1	Olaparib	shared
KCL650	*ATM*	Splice site	Splice variant	1	Olaparib	shared
RMH008	*PIK3CA*	Nonsynonymous SNV	p.E39K	1	Alpelisib	shared
RMH008	*ERBB2*	Nonsynonymous SNV	p.L755S	3A	Neratinib	shared
RMH011	*ERBB2*	Amplification	Amplification	1	Trastuzumab	shared

Supplementary Table 6 | Immunohistochemical scoring of primary tumours and matched BCLM PDOs

	Primary tumour	BCLM PDO
KCL320	ER 8; HER2 0	ER 0; HER2 3+
KCL450	ER 8; HER2 0	ER 0; HER2 1+
KCL566	ER 6; HER2 0	ER 3; HER2 2+
KCL622	ER 0; HER2 0	ER 0; HER2 0
KCL625	ER 3; HER2 0	ER 0; HER2 1+

Scoring performed by independent pathologist (I.R.)

Supplementary Table 7 | Antibodies used for immunohistochemistry

Antibody	Species	Source (Catalogue no.)	Dilution
Alpha-catenin	Rabbit	Abcam (51032)	1:100
Beta-catenin	Mouse	BD Biosciences (610153)	1:2500
E-cadherin	Mouse	Dako (M3612)	1:50
ERα	Rabbit	Dako (M3643)	1:80
HER2	N/A	Dako (SK001)	N/A
Lamin A/C	Rabbit	Abcam (108595)	1:750
p120-catenin	Mouse	BD Biosciences (610134)	1:500

Supplementary Figure 1

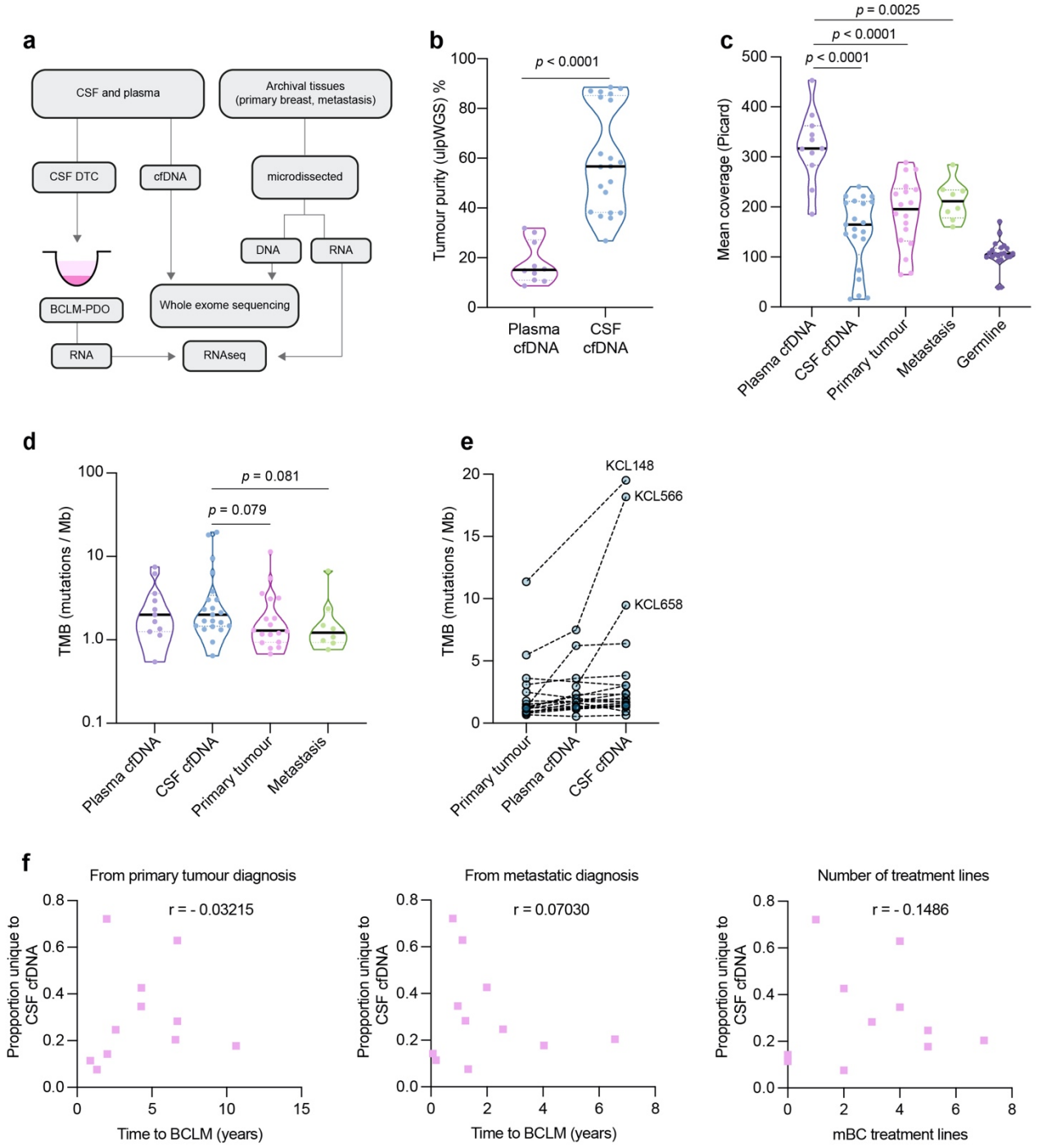

Supplementary Fig. 1. Sequencing pipeline and metrics**. a** Flowchart of sample processing pipeline. DTC, disseminated tumour cell; cfDNA, cell-free DNA; PDO, patient derived organoids. **b** Tumour purity of cfDNA assessed by ulpWGS (ultra-low-pass whole genome sequencing) within the concurrently collected CSF (n = 21) and plasma (n = 11) samples. The 10 plasma cfDNA samples which did not undergo WES (due to tumour content <10%) are not shown. Significance by Mann-Whitney test. **c** Sequencing coverage of all samples. Plasma cfDNA, n = 11; CSF cfDNA, n = 21; primary tumour, n = 18; metastasis, n = 8; germline, n = 21. Significance by Mann-Whitney test. **d** Tumour mutational burden (TMB) in samples shown in panel c. Significance by Mann-Whitney test, p-values <0.1 shown. **e** Matched comparison of TMB in primary tumour, plasma cfDNA and CSF cfDNA samples collected from individual patients. **f** Correlation of proportion of variants unique to CSF cfDNA *vs*. matched plasma cfDNA to time from primary tumour diagnosis (left panel), time from diagnosis of metastatic breast cancer (middle panel), and number of previous systemic therapies (treatment lines) completed (right panel). Pearson's r correlation.

Supplementary Figure 2

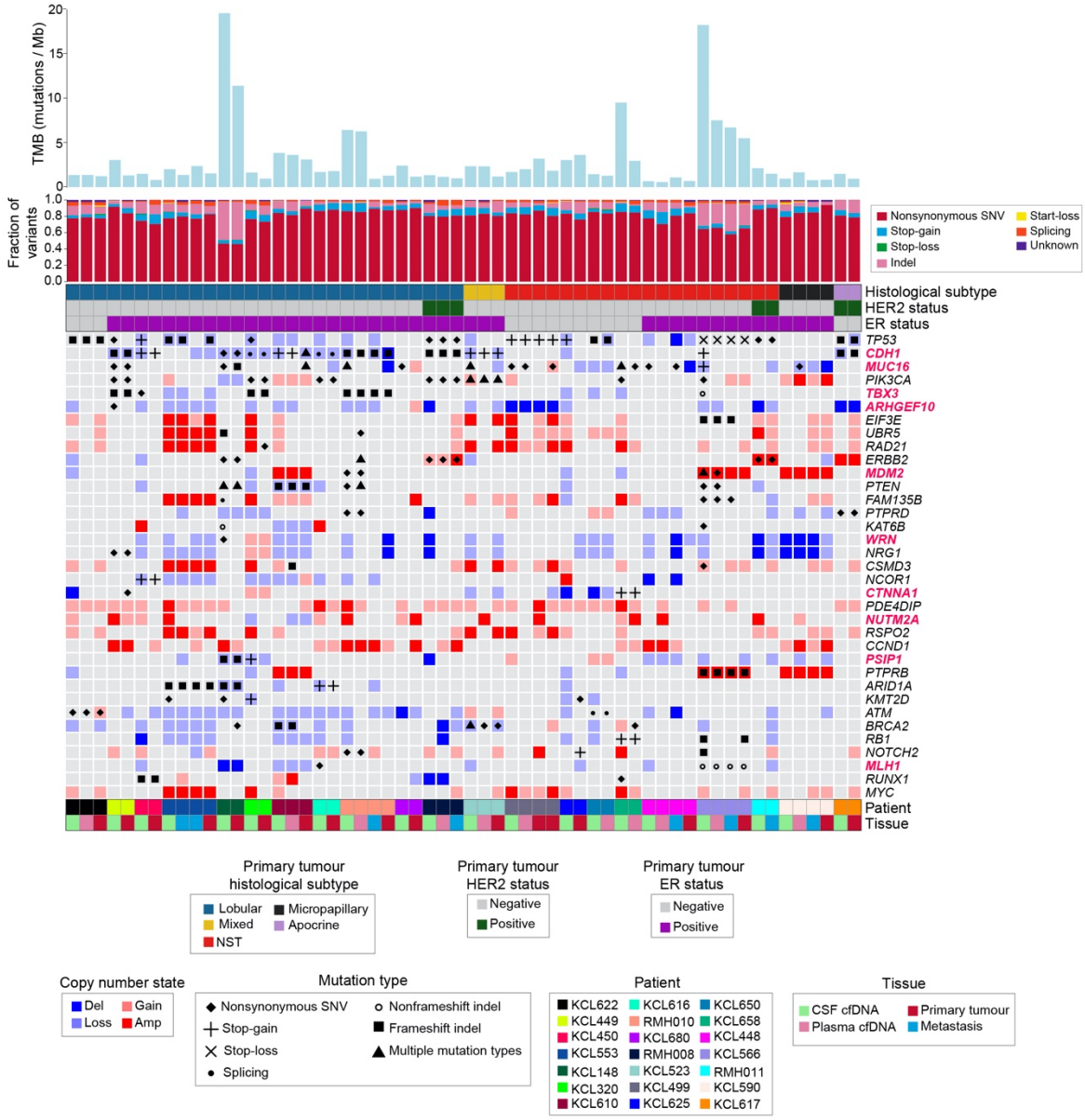

Supplementary Fig. 2 Cancer-associated mutation and copy number landscape of all matched samples. Extended data associated with Fig. 2. Uppermost bar plot show tumour mutational burden (TMB) by sample. Stacked bar chart below shows mutational subtype for each sample as percentage of all variants (excluding synonymous). Banners indicate primary tumour histological subtype and HER2 and ER status. Main plot shows the 36 most frequently cancer-associated altered genes (alterations include mutation and high-level copy number events) in CSF cfDNA as follows; Cancer Gene Census (CGC) gene altered in at least 4 cases; breast cancer driver gene (definition in Methods) altered in at least 3 cases. Gene names are highlighted in red if genetic alteration rate was significantly different ($p \leq 0.05$ by Chi-square test) to publicly-available dataset of 216 metastatic breast cancer (MBC) samples (see Methods).

Supplementary Figure 3

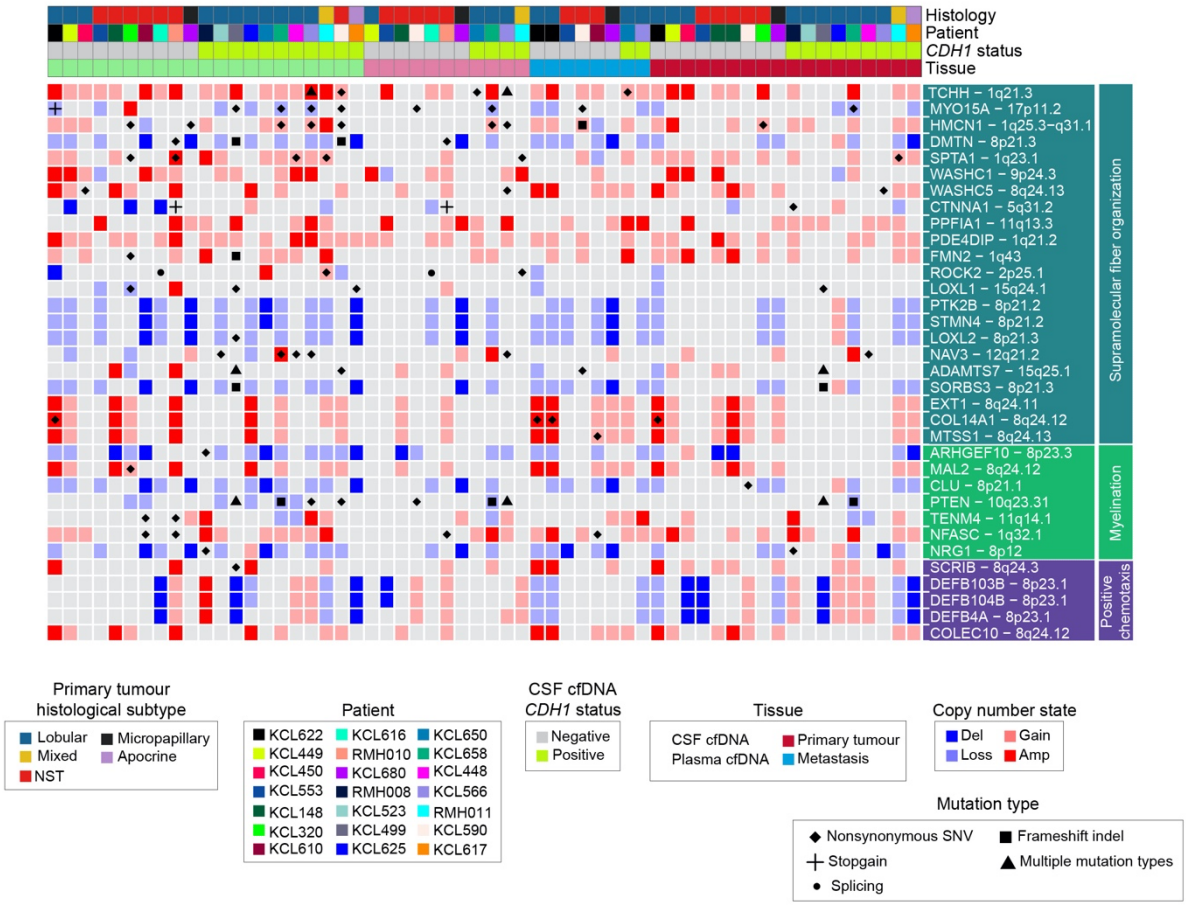

Supplementary Fig. 3. BCLM enriched biological processes. Associated with Fig. 3b. Focused alteration plot of genes from GO biological processes with -$\log_{10}$ p-value ≥3.0 in CSF cfDNA *vs*. plasma cfDNA. Genetic alterations are shown for all sample types in 21 individuals. Banners above indicate; primary tumour histological subtype, patients, *CDH1* mutation status of CSF cfDNA and tissue type.

Supplementary Figure 4

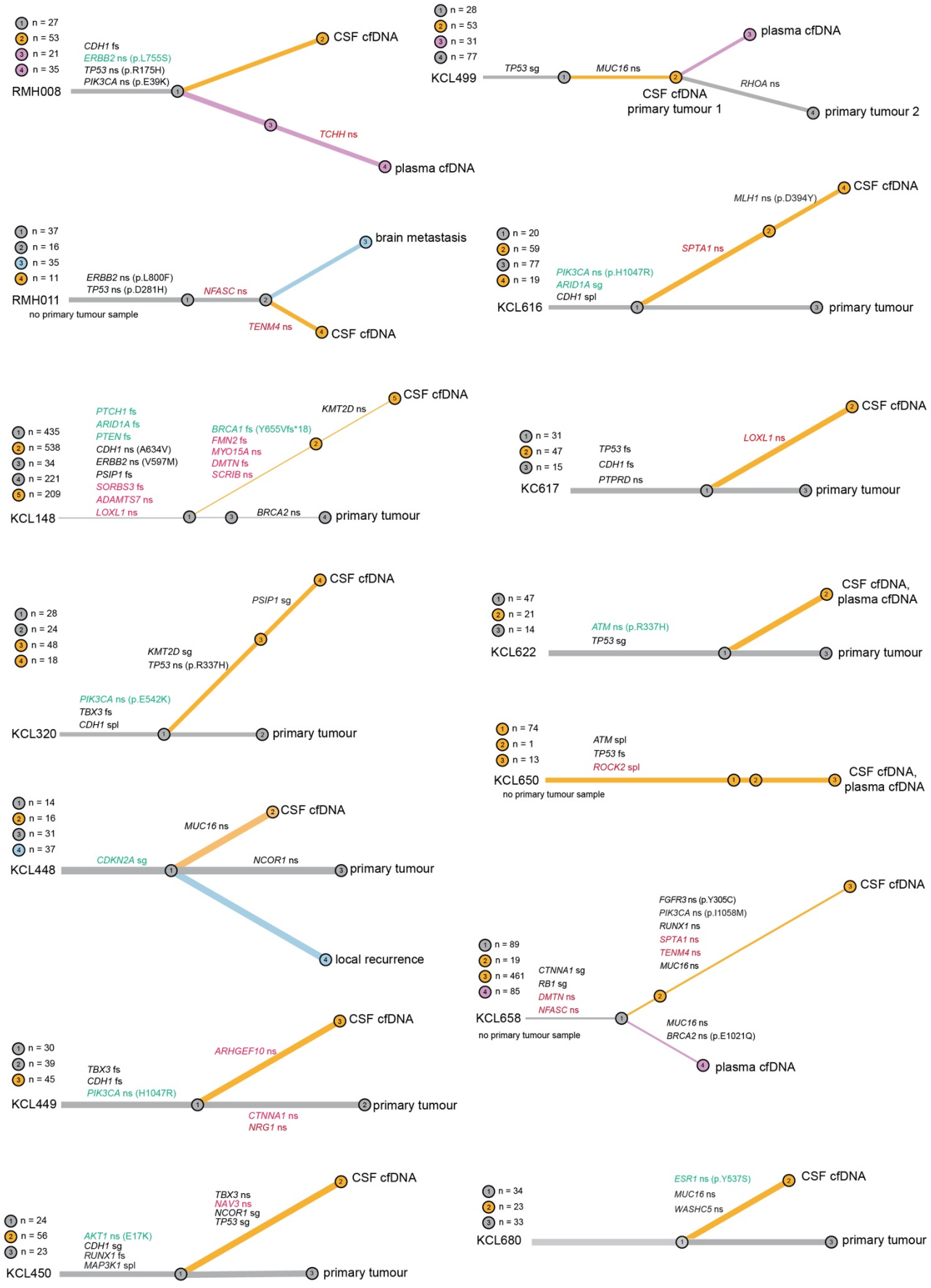

Supplementary Fig. 4. BCLM subclone evolution. Associated with Fig. 3c. Phylogenetic trees depicting BCLM genetic evolution. ClonEvol was used to infer consensus clonal evolution models, using the variant clusters and cellular prevalence generated by PyClone. Each branch represents the evolution path of a clone from its parental clone, and each node marks the clone number of the preceding branch. Samples are annotated at clone nodes when no further subclone evolution occurs. Branch lengths are scaled by the square root of number of mutations per clone, and branch width is inversely proportional to branch length. Mutations per clone number are shown to top left of the trees. Gene names and variant type are annotated on branches as follows; black font if appear in list of commonly altered cancer driver genes (Fig. 2 and/or a breast cancer driver (defined in Methods)); green font if variant is OncoKB annotated as therapeutically actionable (Supplementary Table 5); red font are genes altered in CSF-enriched GO biological processes (see Fig. 3b). Variant type abbreviations; fs, frameshift; ns, non-synonymous; sg, stop-gain; spl, splice-site variant; .

Supplementary Figure 5

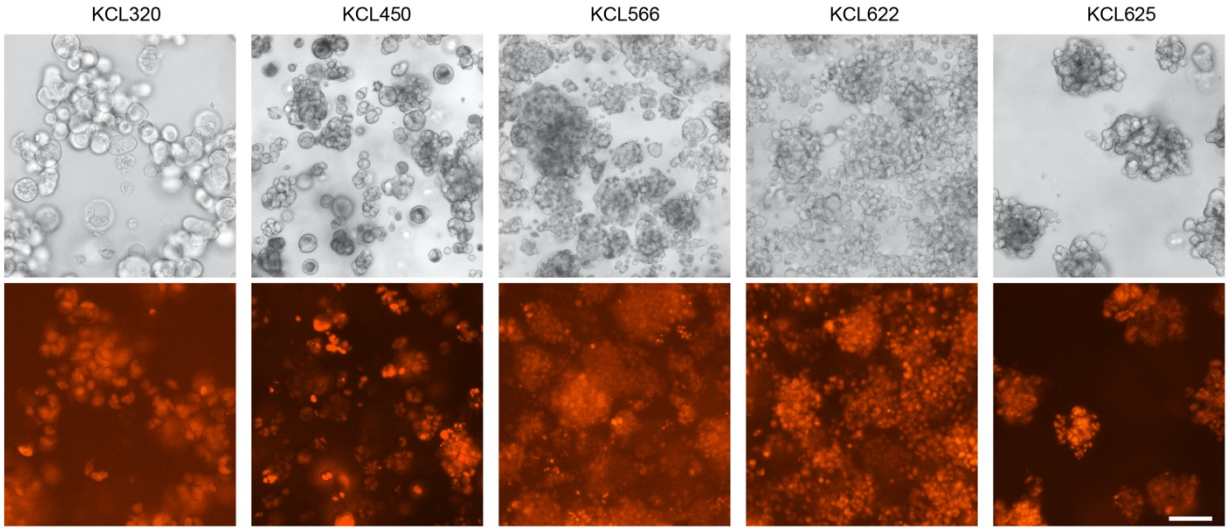

Supplementary Fig. 5. Tagging BCLM patient-derived organoids. PDOs were transduced with a lentivirus encoding luciferase and mCherry (mChLuc2) and imaged on an EVOS microscope in bright field and fluorescence mode. Scale bar, 100 µm

Supplementary Table 4 | Genetic alterations in BCLM vs. MBC cohort

Gene	BCLM mutated	BCLM deleted	BCLM amplified	BCLM total altered	BCLM total profiled	MBC mutated	MBC deleted	MBC amplified	MBC total altered	MBC total profiled	Proportion test (*p* value)
AKT1	1	0	1	2	21	10	1	5	16	216	1.000
AKT2	0	0	1	1	21	2	0	7	9	216	1.000
APC	0	0	0	0	21	4	0	1	5	216	1.000
ARID1A	3	0	0	3	21	8	3	1	12	216	0.272
ARID1B	0	0	0	0	21	4	0	2	6	216	0.963
ASXL1	0	0	0	0	21	6	0	6	12	216	0.557
ATM	2	1	0	3	21	8	5	0	13	216	0.324
ATR	0	0	0	0	21	3	2	1	6	216	0.963
AXIN1	0	0	0	0	21	0	0	17	17	216	0.373
BAP1	1	0	0	1	21	0	1	2	3	216	0.796
BRCA1	1	1	0	2	21	2	5	3	10	216	0.649
BRCA2	2	0	0	2	21	7	0	2	9	216	0.568
BUB1B	0	0	0	0	21	2	3	0	5	216	1.000
CASP8	0	0	0	0	21	0	1	3	4	216	1.000
CBFB	0	0	0	0	21	7	0	4	11	216	0.606
CBLB	1	0	0	1	21	0	2	10	12	216	1.000
CDH1	11	0	0	11	21	16	1	0	17	216	0.000
CDKN1B	1	0	0	1	21	3	1	2	6	216	1.000
CDKN2A	1	0	1	2	21	4	5	5	14	216	0.940
CHEK2	0	0	0	0	21	3	4	2	9	216	0.722
CIC	2	0	0	2	21	3	3	7	13	216	0.873
CNOT3	0	0	1	1	21	1	2	12	15	216	1.000
CREBBP	1	0	0	1	21	1	0	3	4	216	0.928
CTCF	0	0	0	0	21	5	2	4	11	216	0.606
CTNNA1	1	3	0	4	21	0	1	1	2	216	0.000
CUX1	2	0	0	2	21	3	1	2	6	216	0.317
DNMT3A	1	0	0	1	21	0	0	1	1	216	0.420
ECT2L	0	0	0	0	21	5	1	5	11	216	0.606
EGFR	1	0	0	1	21	3	1	13	17	216	0.935
ERBB2	3	0	2	5	21	7	1	19	27	216	0.266
ERBB3	0	0	0	0	21	3	1	2	6	216	0.963
ERCC4	0	0	0	0	21	2	0	4	6	216	0.963
ESR1	1	0	0	1	21	23	0	9	32	216	0.347
FBXW7	0	0	0	0	21	4	2	8	14	216	0.473
FGFR2	1	0	0	1	21	1	1	5	7	216	1.000
FOXO3	1	1	0	2	21	1	2	5	8	216	0.485
FOXP1	1	0	0	1	21	5	2	3	10	216	1.000
GATA3	1	0	0	1	21	28	0	10	38	216	0.228
GNAS	1	0	0	1	21	1	0	24	25	216	0.557
GPS2	0	0	0	0	21	3	0	4	7	216	0.871
HRAS	1	0	0	1	21	2	2	7	11	216	1.000
KMT2D	3	0	0	3	21	10	0	1	11	216	0.222
KRAS	1	0	0	1	21	3	2	10	15	216	1.000
MAP2K4	0	1	0	1	21	10	3	0	13	216	1.000
MAP3K1	2	0	0	2	21	24	2	0	26	216	1.000
MED23	1	0	0	1	21	5	1	6	12	216	1.000
MEN1	1	0	0	1	21	3	2	4	9	216	1.000
MLH1	2	1	0	3	21	3	0	1	4	216	0.011
MSH2	1	0	0	1	21	0	1	1	2	216	0.632
NCOR1	1	1	1	3	21	6	2	0	8	216	0.097
NF1	1	0	0	1	21	13	2	3	18	216	0.877
NF2	1	0	0	1	21	1	0	3	4	216	0.928
NOTCH1	1	0	0	1	21	1	1	6	8	216	1.000
NOTCH2	2	0	1	3	21	6	0	9	15	216	0.435
NRAS	0	0	0	0	21	0	0	1	1	216	1.000
PALB2	0	0	0	0	21	8	0	2	10	216	0.661
PBRM1	1	0	0	1	21	4	3	0	7	216	1.000
PIK3CA	7	0	0	7	21	75	0	6	81	216	0.888
PIK3R1	1	0	0	1	21	7	2	7	16	216	0.996
PMS2	0	0	0	0	21	0	3	2	5	216	1.000
PRDM1	0	0	0	0	21	3	2	7	12	216	0.557
PREX2	1	0	0	1	21	7	2	27	36	216	0.263
PTEN	4	0	0	4	21	9	5	3	17	216	0.187
RB1	2	1	0	3	21	11	2	1	14	216	0.379
RHOA	1	0	0	1	21	2	10	1	13	216	1.000
RUNX1	2	1	0	3	21	1	1	6	8	216	0.097
SETD2	0	0	0	0	21	6	2	0	8	216	0.792
SF3B1	0	0	0	0	21	3	1	1	5	216	1.000
SMAD4	0	0	0	0	21	3	5	1	9	216	0.722
SMARCA4	2	0	0	2	21	5	1	5	11	216	0.727
SPEN	2	0	0	2	21	12	2	2	16	216	1.000
STK11	1	0	0	1	21	2	2	8	12	216	1.000
TBL1XR1	0	0	0	0	21	2	0	12	14	216	0.473
TBX3	5	0	0	5	21	8	1	1	10	216	0.003
TET2	1	0	0	1	21	2	2	3	7	216	1.000
TP53	12	0	0	12	21	87	5	3	95	216	0.354
XBP1	0	0	0	0	21	2	1	4	7	216	0.871
A1CF	1	0	1	2	21	1	0	8	9	216	0.568
ABI1	0	0	0	0	21	4	0	1	5	216	1.000
ABL1	1	0	0	1	21	1	1	1	3	216	0.796
ABL2	1	0	0	1	21	2	0	1	3	216	0.796
ACKR3	0	0	0	0	21	0	4	3	7	216	0.871
ACSL3	0	0	0	0	21	3	1	3	7	216	0.871
ACVR1	0	0	0	0	21	2	1	4	7	216	0.871
ACVR2A	1	0	0	1	21	1	2	5	8	216	1.000
AFF1	1	0	0	1	21	2	2	0	4	216	0.928
AKAP9	1	0	0	1	21	6	2	5	13	216	1.000
AKT3	1	0	1	2	21	1	0	19	20	216	1.000
ALK	1	0	0	1	21	7	0	1	8	216	1.000
ANK1	2	1	0	3	21	3	1	15	19	216	0.664
ARHGAP26	2	0	0	2	21	0	0	1	1	216	0.012
ARHGAP5	0	0	2	2	21	5	0	8	13	216	0.873
ARHGEF10	1	4	0	5	21	1	2	4	7	216	0.000
ARHGEF10L	0	0	0	0	21	1	2	0	3	216	1.000
ARHGEF12	0	0	0	0	21	5	3	0	8	216	0.792
ARID2	0	0	0	0	21	5	2	5	12	216	0.557
ARNT	2	0	1	3	21	1	0	10	11	216	0.222
ASPSCR1	0	0	0	0	21	0	0	18	18	216	0.345
ATF1	0	0	0	0	21	0	1	0	1	216	1.000
ATIC	1	0	0	1	21	1	0	1	2	216	0.632
ATP1A1	1	0	0	1	21	2	0	3	5	216	1.000
AXIN2	0	0	0	0	21	1	0	14	15	216	0.436
B2M	1	0	0	1	21	0	1	0	1	216	0.420
BARD1	0	0	0	0	21	3	0	4	7	216	0.871
BAX	0	0	1	1	21	2	1	5	8	216	1.000
BAZ1A	1	0	1	2	21	2	0	7	9	216	0.568
BCL10	0	1	1	2	21	1	2	2	5	216	0.235
BCL11A	1	0	0	1	21	3	1	3	7	216	1.000
BCL11B	2	0	0	2	21	3	1	3	7	216	0.401
BCL2	0	0	0	0	21	0	2	4	6	216	0.963
BCL2L12	1	0	1	2	21	0	1	7	8	216	0.485
BCL3	0	0	0	0	21	0	1	4	5	216	1.000
BCL6	0	0	0	0	21	2	0	9	11	216	0.606
BCL7A	1	0	0	1	21	0	2	2	4	216	0.928
BCL9	1	0	1	2	21	4	0	20	24	216	1.000
BCL9L	0	0	0	0	21	0	2	2	4	216	1.000
BCLAF1	1	0	0	1	21	0	0	4	4	216	0.928
BCR	0	0	0	0	21	0	0	1	1	216	1.000
BIRC3	0	0	1	1	21	1	5	4	10	216	1.000
BLM	1	0	2	3	21	3	0	1	4	216	0.011
BMPR1A	0	0	0	0	21	1	1	14	16	216	0.403
BRD3	1	0	0	1	21	3	1	4	8	216	1.000
BRD4	1	0	0	1	21	0	1	7	8	216	1.000
BRIP1	0	0	0	0	21	0	1	17	18	216	0.345
BTG1	0	0	1	1	21	0	0	13	13	216	1.000
CACNA1D	0	0	0	0	21	0	2	0	2	216	1.000
CALR	0	1	0	1	21	3	0	7	10	216	1.000
CAMTA1	0	0	0	0	21	1	2	0	3	216	1.000
CANT1	0	0	0	0	21	0	0	9	9	216	0.722
CARD11	0	0	0	0	21	3	2	3	8	216	0.792
CASP3	0	0	0	0	21	0	5	2	7	216	0.871
CASP9	0	0	0	0	21	0	2	0	2	216	1.000
CBFA2T3	0	0	0	0	21	0	1	3	4	216	1.000
CBL	1	0	0	1	21	2	2	1	5	216	1.000
CBLC	0	0	0	0	21	0	1	4	5	216	1.000
CCDC6	0	0	1	1	21	2	0	6	8	216	1.000
CCNB1IP1	0	0	1	1	21	0	1	5	6	216	1.000
CCNC	0	0	0	0	21	2	4	2	8	216	0.792
CCND1	0	0	4	4	21	0	1	52	53	216	0.768
CCND2	0	0	0	0	21	1	1	5	7	216	0.871
CCND3	0	0	0	0	21	1	0	6	7	216	0.871
CCNE1	0	0	0	0	21	0	0	9	9	216	0.722
CCR4	0	0	0	0	21	1	1	0	2	216	1.000
CCR7	0	0	0	0	21	0	0	6	6	216	0.963
CD209	0	0	0	0	21	1	2	4	7	216	0.871
CD274	0	1	0	1	21	0	1	2	3	216	0.796
CD28	0	0	0	0	21	2	0	1	3	216	1.000
CD74	0	0	0	0	21	0	1	1	2	216	1.000
CD79A	1	0	0	1	21	2	0	3	5	216	1.000
CD79B	1	0	0	1	21	0	0	17	17	216	0.935
CDC73	0	0	1	1	21	0	1	30	31	216	0.372
CDH10	0	0	0	0	21	1	2	11	14	216	0.473
CDH11	1	0	0	1	21	0	0	3	3	216	0.796
CDH17	0	0	1	1	21	2	0	21	23	216	0.635

CDK12	1	0	2	3	21	2	5	15	22	216	0.832
CDK4	0	0	0	0	21	0	0	7	7	216	0.871
CDK6	0	0	0	0	21	1	2	13	16	216	0.403
CDKN1A	0	0	0	0	21	0	0	2	2	216	1.000
CDKN2C	0	1	0	1	21	0	1	2	3	216	0.796
CDX2	0	0	0	0	21	0	1	5	6	216	0.963
CEBPA	1	0	0	1	21	1	0	6	7	216	1.000
CEP89	1	0	1	2	21	0	1	4	5	216	0.235
CHCHD7	0	0	0	0	21	0	1	9	10	216	0.661
CHD2	1	0	2	3	21	3	0	5	8	216	0.097
CHD4	0	0	0	0	21	4	0	4	8	216	0.792
CHIC2	0	0	0	0	21	0	0	2	2	216	1.000
CHST11	0	0	1	1	21	1	0	1	2	216	0.632
CIITA	1	0	0	1	21	2	0	6	8	216	1.000
CLIP1	1	0	0	1	21	5	3	0	8	216	1.000
CLP1	0	1	0	1	21	1	0	2	3	216	0.796
CLTC	0	0	0	0	21	2	0	18	20	216	0.296
CLTCL1	1	0	0	1	21	5	1	0	6	216	1.000
CNBD1	1	0	1	2	21	2	0	29	31	216	0.779
CNBP	0	0	0	0	21	0	1	1	2	216	1.000
CNTNAP2	0	0	0	0	21	2	2	6	10	216	0.661
CNTRL	1	0	0	1	21	4	0	1	5	216	1.000
COL1A1	1	0	0	1	21	2	0	19	21	216	0.723
COL2A1	2	0	0	2	21	1	0	3	4	216	0.159
COL3A1	1	0	0	1	21	2	2	13	17	216	0.935
COX6C	0	0	3	3	21	0	1	27	28	216	1.000
CPEB3	0	0	0	0	21	1	3	0	4	216	1.000
CREB1	0	0	0	0	21	0	0	1	1	216	1.000
CREB3L1	0	0	0	0	21	0	0	6	6	216	0.963
CREB3L2	1	0	0	1	21	0	0	1	1	216	0.420
CRNKL1	0	0	0	0	21	3	0	5	8	216	0.792
CRTC1	0	0	0	0	21	0	0	4	4	216	1.000
CRTC3	0	0	2	2	21	2	0	1	3	216	0.093
CSF1R	0	0	0	0	21	1	1	1	3	216	1.000
CSF3R	0	0	0	0	21	2	0	1	3	216	1.000
CSMD3	1	0	3	4	21	12	1	50	63	216	0.466
CTNNA2	1	0	0	1	21	5	1	4	10	216	1.000
CTNNB1	0	0	0	0	21	1	0	4	5	216	1.000
CTNND2	1	0	0	1	21	0	0	8	8	216	1.000
CUL3	0	0	0	0	21	2	1	2	5	216	1.000
CYLD	0	0	0	0	21	1	2	3	6	216	0.963
CYP2C8	1	0	0	1	21	0	2	0	2	216	0.632
CYSLTR2	0	1	0	1	21	1	1	2	4	216	0.928
DAXX	0	0	1	1	21	0	0	4	4	216	0.928
DCC	1	0	0	1	21	6	2	5	13	216	1.000
DDB2	0	0	0	0	21	2	0	4	6	216	0.963
DDIT3	0	0	0	0	21	0	0	2	2	216	1.000
DDR2	0	0	1	1	21	3	0	21	24	216	0.595
DDX10	1	1	0	2	21	2	5	3	10	216	0.649
DDX5	0	0	0	0	21	1	0	18	19	216	0.319
DDX6	0	0	0	0	21	0	3	0	3	216	1.000
DEK	0	0	0	0	21	1	0	1	2	216	1.000
DGCR8	0	0	0	0	21	1	1	3	5	216	1.000
DICER1	0	0	0	0	21	2	2	4	8	216	0.792
DNAJB1	0	0	1	1	21	0	1	4	5	216	1.000
DNM2	0	0	0	0	21	1	1	6	8	216	0.792
DROSHA	2	0	0	2	21	2	1	2	5	216	0.235
EBF1	0	0	0	0	21	2	0	8	10	216	0.661
EED	0	0	1	1	21	0	4	2	6	216	1.000
EIF3E	1	0	4	5	21	0	1	42	43	216	0.888
EIF4A2	0	0	0	0	21	0	1	4	5	216	1.000
ELF3	0	0	2	2	21	2	0	15	17	216	1.000
ELK4	0	0	2	2	21	0	0	13	13	216	0.873
ELL	1	0	0	1	21	0	0	5	5	216	1.000
ELN	1	0	0	1	21	0	1	4	5	216	1.000
EP300	0	0	0	0	21	12	1	0	13	216	0.513
EPAS1	0	0	0	0	21	1	0	1	2	216	1.000
EPHA3	0	0	0	0	21	2	3	10	15	216	0.436
EPHA7	1	0	0	1	21	3	4	11	18	216	0.877
EPS15	0	1	0	1	21	0	0	2	2	216	0.632
ERBB4	1	0	0	1	21	9	1	11	21	216	0.723
ERC1	1	0	0	1	21	3	0	7	10	216	1.000
ERCC2	0	0	0	0	21	2	1	4	7	216	0.871
ERG	0	2	0	2	21	0	0	5	5	216	0.235
ETNK1	1	0	0	1	21	0	3	12	15	216	1.000
ETV1	1	0	0	1	21	0	2	14	16	216	0.996
ETV4	0	1	1	2	21	1	1	4	6	216	0.317
ETV5	0	0	0	0	21	3	1	2	6	216	0.963
ETV6	0	0	0	0	21	0	1	5	6	216	0.963
EWSR1	0	0	0	0	21	0	0	2	2	216	1.000
EXT1	0	0	4	4	21	0	0	43	43	216	1.000
EXT2	0	0	0	0	21	1	0	3	4	216	1.000
EZH2	0	0	0	0	21	3	1	1	5	216	1.000
EZR	1	1	0	2	21	0	0	1	1	216	0.012
FAM131B	1	0	0	1	21	1	1	1	3	216	0.796
FAM135B	2	0	3	5	21	4	1	31	36	216	0.600
FANCA	1	0	0	1	21	2	1	3	6	216	1.000
FANCC	0	0	0	0	21	1	1	0	2	216	1.000
FANCD2	0	0	0	0	21	3	1	5	9	216	0.722
FANCE	0	0	0	0	21	1	0	4	5	216	1.000
FANCF	0	0	1	1	21	2	3	12	17	216	0.935
FANCG	0	0	0	0	21	2	0	3	5	216	1.000
FAS	0	0	0	0	21	1	2	5	8	216	0.792
FAT1	1	0	0	1	21	10	4	2	16	216	0.996
FAT3	1	0	1	2	21	8	4	5	17	216	1.000
FAT4	2	0	0	2	21	6	2	6	14	216	0.940
FBLN2	0	0	0	0	21	4	0	6	10	216	0.661
FBXO11	0	0	0	0	21	2	1	0	3	216	1.000
FCGR2B	0	0	2	2	21	0	0	20	20	216	1.000
FCRL4	0	0	2	2	21	1	1	24	26	216	1.000
FEN1	1	0	0	1	21	0	0	6	6	216	1.000
FES	1	0	2	3	21	1	0	6	7	216	0.066
FEV	0	0	0	0	21	0	0	2	2	216	1.000
FGFR1	0	1	1	2	21	2	1	29	32	216	0.738
FGFR3	1	0	0	1	21	0	2	6	8	216	1.000
FGFR4	0	0	0	0	21	2	1	2	5	216	1.000
FH	0	0	1	1	21	2	0	19	21	216	0.723
FHIT	0	0	0	0	21	0	1	2	3	216	1.000
FIP1L1	0	0	0	0	21	1	0	2	3	216	1.000
FKBP9	0	0	0	0	21	0	0	5	5	216	1.000
FLCN	1	0	1	2	21	1	1	2	4	216	0.159
FLI1	1	0	0	1	21	0	4	4	8	216	1.000
FLT3	0	0	0	0	21	1	1	3	5	216	1.000
FLT4	3	0	0	3	21	2	4	2	8	216	0.097
FNBP1	0	0	0	0	21	4	4	0	8	216	0.792
FOXA1	1	0	0	1	21	10	3	14	27	216	0.487
FOXL2	0	0	0	0	21	0	0	1	1	216	1.000
FOXO1	0	1	0	1	21	1	0	3	4	216	0.928
FOXR1	0	0	0	0	21	2	2	1	5	216	1.000
FSTL3	0	0	0	0	21	1	5	5	11	216	0.606
FUBP1	0	1	0	1	21	0	2	0	2	216	0.632
FUS	0	0	0	0	21	3	0	9	12	216	0.557
GAS7	0	1	0	1	21	0	3	0	3	216	0.796
GATA2	0	0	0	0	21	0	0	2	2	216	1.000
GLI1	2	0	0	2	21	1	1	1	3	216	0.093
GMPS	0	0	0	0	21	1	1	0	2	216	1.000
GNA11	0	0	0	0	21	0	2	5	7	216	0.871
GNAQ	1	0	0	1	21	2	0	1	3	216	0.796
GOLGA5	0	0	0	0	21	2	1	2	5	216	1.000
GOPC	0	0	0	0	21	0	3	7	10	216	0.661
GPC5	0	1	0	1	21	0	2	9	11	216	1.000
GPHN	0	0	0	0	21	0	1	0	1	216	1.000
GRIN2A	0	0	0	0	21	5	0	5	10	216	0.661
GRM3	0	0	0	0	21	4	2	14	20	216	0.296
HERPUD1	0	0	0	0	21	0	0	1	1	216	1.000
HEY1	0	0	0	0	21	1	0	24	25	216	0.202
HIF1A	1	0	0	1	21	1	0	1	2	216	0.632
HIP1	0	0	0	0	21	3	0	3	6	216	0.963
HLA-A	1	0	0	1	21	0	0	4	4	216	0.928
HLF	0	0	0	0	21	0	0	14	14	216	0.473
HMGA1	0	0	0	0	21	0	0	3	3	216	1.000
HMGA2	0	0	2	2	21	0	1	6	7	216	0.401
HMGN2P46	0	0	0	0	21	0	2	0	2	216	1.000
HNF1A	1	0	0	1	21	0	0	1	1	216	0.420
HNRNPA2B1	0	0	0	0	21	1	1	5	7	216	0.871
HOOK3	0	0	0	0	21	2	3	12	17	216	0.373
HOXA11	1	0	0	1	21	0	0	9	9	216	1.000
HOXA13	0	0	0	0	21	0	0	7	7	216	0.871
HOXC11	0	0	0	0	21	1	1	3	5	216	1.000
HOXC13	0	0	0	0	21	0	1	2	3	216	1.000
HOXD11	0	0	0	0	21	0	0	1	1	216	1.000
HOXD13	0	0	0	0	21	0	0	1	1	216	1.000
HSP90AA1	1	1	0	2	21	3	1	2	6	216	0.317
HSP90AB1	0	0	0	0	21	3	0	7	10	216	0.661
ID3	0	0	0	0	21	0	0	1	1	216	1.000
IDH1	0	0	0	0	21	1	0	1	2	216	1.000
IDH2	1	0	2	3	21	0	0	7	7	216	0.066
IGF2BP2	1	0	0	1	21	0	1	2	3	216	0.796
IKBKB	0	1	0	1	21	1	2	13	16	216	0.996
IKZF1	1	0	0	1	21	2	0	13	15	216	1.000

IL2	0	0	0	0	21	0	2	2	4	216	1.000
IL21R	0	0	0	0	21	1	0	5	6	216	0.963
IL6ST	0	0	0	0	21	2	1	0	3	216	1.000
IL7R	0	0	0	0	21	1	1	9	11	216	0.606
IRF4	1	0	0	1	21	0	2	5	7	216	1.000
ISX	0	0	0	0	21	0	1	1	2	216	1.000
ITGAV	0	0	0	0	21	0	1	6	7	216	0.871
JAK1	2	0	0	2	21	3	2	4	9	216	0.568
JAK2	0	1	0	1	21	1	1	3	5	216	1.000
JAK3	1	0	0	1	21	1	1	4	6	216	1.000
JAZF1	0	0	0	0	21	2	0	12	14	216	0.473
JUN	0	0	0	0	21	1	1	8	10	216	0.661
KAT6A	0	1	0	1	21	2	2	15	19	216	0.823
KAT6B	2	0	2	4	21	2	0	10	12	216	0.058
KAT7	1	0	0	1	21	3	0	12	15	216	1.000
KCNJ5	1	0	0	1	21	0	5	2	7	216	1.000
KDM5A	0	0	0	0	21	1	1	9	11	216	0.606
KDR	1	0	0	1	21	2	0	3	5	216	1.000
KDSR	0	0	0	0	21	0	2	4	6	216	0.963
KEAP1	0	0	0	0	21	5	2	6	13	216	0.513
KIAA1549	0	0	0	0	21	1	0	1	2	216	1.000
KIF5B	0	0	0	0	21	0	2	1	3	216	1.000
KIT	1	0	0	1	21	4	0	4	8	216	1.000
KLF4	0	0	0	0	21	3	1	0	4	216	1.000
KLF6	0	0	0	0	21	1	0	10	11	216	0.606
KLK2	0	0	1	1	21	0	1	5	6	216	1.000
KMT2A	1	0	0	1	21	9	2	0	11	216	1.000
KMT2C	1	0	0	1	21	14	1	0	15	216	1.000
KNSTRN	0	0	0	0	21	0	2	3	5	216	1.000
KTN1	0	0	0	0	21	0	2	5	7	216	0.871
LARP4B	0	0	0	0	21	1	1	8	10	216	0.661
LASP1	0	0	2	2	21	2	1	7	10	216	0.649
LCK	1	0	0	1	21	1	0	3	4	216	0.928
LCP1	1	1	0	2	21	2	0	2	4	216	0.159
LEF1	1	0	0	1	21	1	2	1	4	216	0.928
LEPROTL1	0	3	0	3	21	0	3	2	5	216	0.023
LIFR	0	0	0	0	21	2	1	9	12	216	0.557
LMNA	0	0	2	2	21	1	0	15	16	216	1.000
LMO1	0	0	0	0	21	0	3	1	4	216	1.000
LMO2	0	0	0	0	21	0	0	8	8	216	0.792
LPP	1	0	0	1	21	0	0	9	9	216	1.000
LRIG3	0	0	0	0	21	1	0	14	15	216	0.436
LRP1B	2	0	0	2	21	7	3	8	18	216	1.000
LSM14A	0	0	0	0	21	0	0	4	4	216	1.000
LYL1	0	0	0	0	21	0	0	7	7	216	0.871
LZTR1	0	0	0	0	21	4	1	3	8	216	0.792
MAF	0	0	0	0	21	0	1	2	3	216	1.000
MAFB	0	0	0	0	21	0	1	5	6	216	0.963
MALAT1	0	3	0	3	21	0	0	8	8	216	0.097
MALT1	0	0	0	0	21	0	1	1	2	216	1.000
MAML2	0	0	1	1	21	4	4	4	12	216	1.000
MAP2K1	0	0	1	1	21	1	0	1	2	216	0.632
MAP2K2	0	0	0	0	21	0	2	4	6	216	0.963
MAP3K13	0	0	0	0	21	3	1	2	6	216	0.963
MAPK1	1	0	0	1	21	3	1	1	5	216	1.000
MAX	0	0	0	0	21	2	0	1	3	216	1.000
MB21D2	0	0	0	0	21	2	1	13	16	216	0.403
MDM2	2	0	3	5	21	2	0	10	12	216	0.008
MDM4	1	0	2	3	21	1	0	13	14	216	0.379
MECOM	1	0	1	2	21	4	1	21	26	216	1.000
MET	1	0	0	1	21	2	0	5	7	216	1.000
MGMT	0	0	0	0	21	0	3	1	4	216	1.000
MITF	0	0	0	0	21	2	1	3	6	216	0.963
MLF1	1	0	0	1	21	0	1	5	6	216	1.000
MLLT1	0	0	0	0	21	0	2	6	8	216	0.792
MLLT10	0	0	0	0	21	2	0	1	3	216	1.000
MLLT11	0	0	1	1	21	1	0	9	10	216	1.000
MLLT3	1	0	1	2	21	1	1	4	6	216	0.317
MLLT6	0	0	2	2	21	1	1	11	13	216	0.873
MN1	1	0	0	1	21	0	0	2	2	216	0.632
MNX1	0	0	0	0	21	0	1	0	1	216	1.000
MPL	0	0	0	0	21	0	0	4	4	216	1.000
MSH6	0	0	0	0	21	1	1	0	2	216	1.000
MSI2	0	0	0	0	21	0	0	11	11	216	0.606
MTOR	0	0	0	0	21	5	2	0	7	216	0.871
MUC1	0	0	1	1	21	2	0	23	25	216	0.557
MUC16	9	0	0	9	21	19	1	1	21	216	0.000
MUC4	1	1	0	2	21	8	0	5	13	216	0.873
MUTYH	0	0	0	0	21	1	0	5	6	216	0.963
MYB	1	0	0	1	21	3	0	6	9	216	1.000
MYC	0	0	4	4	21	0	0	41	41	216	1.000
MYCL	0	0	0	0	21	1	0	5	6	216	0.963
MYCN	2	0	1	3	21	2	2	2	6	216	0.042
MYD88	0	1	0	1	21	0	0	2	2	216	0.632
MYH11	2	0	0	2	21	7	0	3	10	216	0.649
MYH9	1	0	0	1	21	3	0	1	4	216	0.928
MYO5A	0	0	0	0	21	6	1	2	9	216	0.722
MYOD1	0	0	0	0	21	1	1	4	6	216	0.963
N4BP2	1	0	0	1	21	2	5	1	8	216	1.000
NAB2	1	0	0	1	21	0	1	2	3	216	0.796
NACA	0	0	0	0	21	2	4	0	6	216	0.963
NBEA	0	1	0	1	21	4	2	6	12	216	1.000
NBN	0	0	1	1	21	1	0	33	34	216	0.302
NCKIPSD	0	0	0	0	21	2	3	2	7	216	0.871
NCOA2	0	0	0	0	21	1	0	15	16	216	0.403
NCOA4	0	0	0	0	21	2	0	1	3	216	1.000
NCOR2	0	0	0	0	21	1	0	6	7	216	0.871
NDRG1	0	0	3	3	21	1	0	43	44	216	0.703
NFATC2	1	0	1	2	21	1	0	12	13	216	0.873
NFE2L2	0	0	0	0	21	1	1	2	4	216	1.000
NFIB	1	1	0	2	21	2	2	9	13	216	0.873
NFKB2	0	0	0	0	21	0	0	3	3	216	1.000
NFKBIE	0	0	0	0	21	0	0	5	5	216	1.000
NIN	1	0	0	1	21	3	0	5	8	216	1.000
NKX2-1	0	0	0	0	21	1	1	7	9	216	0.722
NPM1	0	0	0	0	21	0	1	1	2	216	1.000
NR4A3	0	0	0	0	21	0	0	1	1	216	1.000
NRG1	1	3	0	4	21	4	3	11	18	216	0.222
NSD1	0	0	0	0	21	3	1	0	4	216	1.000
NT5C2	0	0	0	0	21	0	1	0	1	216	1.000
NTHL1	0	0	0	0	21	0	0	16	16	216	0.403
NTRK1	1	0	2	3	21	0	0	17	17	216	0.549
NTRK3	0	0	2	2	21	2	0	9	11	216	0.727
NUMA1	0	0	0	0	21	4	0	5	9	216	0.722
NUP214	2	0	0	2	21	1	1	0	2	216	0.042
NUP98	1	0	0	1	21	5	4	0	9	216	1.000
NUTM1	0	0	0	0	21	1	4	2	7	216	0.871
NUTM2A	0	0	4	4	21	0	1	0	1	216	0.000
OLIG2	0	0	0	0	21	0	0	3	3	216	1.000
PABPC1	0	0	3	3	21	2	0	23	25	216	0.989
PAFAH1B2	1	1	0	2	21	0	1	1	2	216	0.042
PAX3	2	0	0	2	21	3	0	1	4	216	0.159
PAX5	0	0	0	0	21	3	0	2	5	216	1.000
PAX7	0	1	0	1	21	0	2	0	2	216	0.632
PAX8	0	0	0	0	21	2	0	1	3	216	1.000
PBX1	0	0	1	1	21	2	0	19	21	216	0.723
PCBP1	1	0	0	1	21	0	1	0	1	216	0.420
PCM1	1	2	0	3	21	3	3	4	10	216	0.176
PDCD1LG2	1	1	0	2	21	1	1	2	4	216	0.159
PDE4DIP	0	0	4	4	21	1	0	11	12	216	0.058
PDGFB	1	0	0	1	21	0	1	1	2	216	0.632
PDGFRA	1	0	0	1	21	0	0	3	3	216	0.796
PDGFRB	0	0	0	0	21	2	1	1	4	216	1.000
PER1	0	0	0	0	21	0	0	4	4	216	1.000
PHOX2B	0	1	0	1	21	0	3	2	5	216	1.000
PICALM	0	0	1	1	21	0	4	2	6	216	1.000
PIK3CB	1	0	0	1	21	2	0	1	3	216	0.796
PIM1	0	0	0	0	21	0	0	3	3	216	1.000
PLAG1	0	0	0	0	21	1	1	9	11	216	0.606
PLCG1	0	0	0	0	21	5	1	6	12	216	0.557
PML	0	0	1	1	21	0	0	3	3	216	0.796
PMS1	0	0	0	0	21	4	1	2	7	216	0.871
POLD1	1	0	1	2	21	2	1	7	10	216	0.649
POLE	0	0	0	0	21	2	2	1	5	216	1.000
POLG	0	0	2	2	21	0	0	5	5	216	0.235
POLQ	0	0	0	0	21	4	4	0	8	216	0.792
POT1	1	0	0	1	21	0	2	15	17	216	0.935
POU2AF1	1	1	0	2	21	0	2	2	4	216	0.159
POU5F1	0	0	0	0	21	0	0	5	5	216	1.000
PPARG	0	0	0	0	21	3	0	5	8	216	0.792
PPFIBP1	1	0	0	1	21	1	2	9	12	216	1.000
PPM1D	0	0	0	0	21	0	0	16	16	216	0.403
PPP2R1A	0	0	1	1	21	2	1	5	8	216	1.000
PPP6C	0	0	0	0	21	1	3	0	4	216	1.000
PRCC	0	0	2	2	21	0	0	12	12	216	0.801
PRDM16	1	0	0	1	21	0	1	2	3	216	0.796
PRDM2	0	0	0	0	21	3	2	0	5	216	1.000
PRF1	0	0	0	0	21	1	0	5	6	216	0.963
PRKACA	0	0	0	0	21	0	1	5	6	216	0.963
PRKAR1A	0	0	0	0	21	1	0	22	23	216	0.235

PRPF40B	0	0	0	0	21	2	0	3	5	216	1.000
PRRX1	0	0	1	1	21	0	0	20	20	216	0.772
PSIP1	2	1	0	3	21	2	3	1	6	216	0.042
PTCH1	2	0	0	2	21	5	1	0	6	216	0.317
PTK6	1	0	0	1	21	1	0	28	29	216	0.426
PTPN11	0	0	0	0	21	1	1	0	2	216	1.000
PTPN13	0	0	0	0	21	4	3	1	8	216	0.792
PTPN6	0	0	0	0	21	1	0	6	7	216	0.871
PTPRB	1	0	3	4	21	4	1	19	24	216	0.471
PTPRC	1	0	2	3	21	1	1	45	47	216	0.602
PTPRD	2	1	0	3	21	4	2	8	14	216	0.379
PTPRK	0	0	0	0	21	2	1	14	17	216	0.373
PTPRT	0	0	0	0	21	1	1	13	15	216	0.436
QKI	0	0	0	0	21	1	2	5	8	216	0.792
RABEP1	0	0	0	0	21	3	1	0	4	216	1.000
RAC1	0	0	0	0	21	0	2	2	4	216	1.000
RAD17	0	0	0	0	21	0	4	0	4	216	1.000
RAD21	0	0	6	6	21	0	0	48	48	216	0.697
RAD51B	0	0	0	0	21	0	2	0	2	216	1.000
RAF1	0	0	0	0	21	2	0	4	6	216	0.963
RALGDS	0	0	0	0	21	0	1	3	4	216	1.000
RANBP2	1	0	0	1	21	2	1	1	4	216	0.928
RAP1GDS1	0	0	0	0	21	1	4	1	6	216	0.963
RARA	0	0	0	0	21	1	1	10	12	216	0.557
RBM15	1	0	0	1	21	1	0	2	3	216	0.796
RECQL4	0	0	3	3	21	1	0	47	48	216	0.571
REL	0	0	0	0	21	1	2	0	3	216	1.000
RET	0	0	0	0	21	2	1	3	6	216	0.963
RFWD3	0	0	0	0	21	0	1	1	2	216	1.000
RGPD3	0	0	0	0	21	0	0	1	1	216	1.000
RGS7	0	0	1	1	21	1	1	16	18	216	0.877
RHOH	0	0	0	0	21	0	5	1	6	216	0.963
RMI2	0	0	0	0	21	0	0	4	4	216	1.000
RNF213	1	0	0	1	21	6	0	6	12	216	1.000
RNF43	0	0	0	0	21	1	0	13	14	216	0.473
ROBO2	1	0	0	1	21	2	4	10	16	216	0.996
ROS1	2	0	0	2	21	2	3	7	12	216	0.801
RPL22	1	0	0	1	21	0	2	2	4	216	0.928
RPL5	1	0	0	1	21	2	3	1	6	216	1.000
RPN1	0	0	0	0	21	1	0	1	2	216	1.000
RSPO2	0	0	4	4	21	1	1	42	44	216	1.000
RSPO3	0	0	0	0	21	2	2	10	14	216	0.473
RUNX1T1	1	0	1	2	21	2	0	33	35	216	0.624
S100A7	0	0	1	1	21	0	0	15	15	216	1.000
SALL4	0	0	1	1	21	1	0	9	10	216	1.000
SBDS	0	0	0	0	21	2	1	1	4	216	1.000
SDC4	0	0	0	0	21	0	0	9	9	216	0.722
SDHA	0	0	0	0	21	0	1	7	8	216	0.792
SDHAF2	0	0	0	0	21	0	0	5	5	216	1.000
SDHB	1	0	0	1	21	0	2	1	3	216	0.796
SDHC	0	0	1	1	21	0	0	12	12	216	1.000
SDHD	0	1	0	1	21	1	2	0	3	216	0.796
SET	0	0	0	0	21	1	4	1	6	216	0.963
SETBP1	0	0	0	0	21	2	0	7	9	216	0.722
SETD1B	2	0	0	2	21	3	1	4	8	216	0.485
SFPQ	0	1	0	1	21	0	3	1	4	216	0.928
SFRP4	0	0	0	0	21	1	0	14	15	216	0.436
SGK1	0	0	0	0	21	0	1	4	5	216	1.000
SH2B3	0	0	0	0	21	0	0	2	2	216	1.000
SH3GL1	0	0	0	0	21	0	2	4	6	216	0.963
SIRPA	2	0	0	2	21	2	0	4	6	216	0.317
SIX1	0	0	0	0	21	0	0	2	2	216	1.000
SIX2	0	0	0	0	21	1	1	2	4	216	1.000
SKI	1	0	0	1	21	0	2	3	5	216	1.000
SLC34A2	1	0	0	1	21	0	4	0	4	216	0.928
SLC45A3	0	0	2	2	21	3	0	13	16	216	1.000
SMAD2	0	0	0	0	21	0	0	1	1	216	1.000
SMAD3	0	0	1	1	21	1	0	4	5	216	1.000
SMARCB1	0	0	0	0	21	0	0	3	3	216	1.000
SMARCD1	0	0	0	0	21	0	0	3	3	216	1.000
SMARCE1	0	0	0	0	21	2	1	5	8	216	0.792
SMO	0	0	0	0	21	4	0	2	6	216	0.963
SND1	1	0	0	1	21	4	0	6	10	216	1.000
SOCS1	0	0	0	0	21	0	0	4	4	216	1.000
SOX2	0	0	0	0	21	1	1	5	7	216	0.871
SOX21	0	0	0	0	21	1	2	4	7	216	0.871
SPECC1	1	0	0	1	21	1	0	1	2	216	0.632
SPOP	0	0	0	0	21	1	0	11	12	216	0.557
SRC	0	0	0	0	21	4	1	8	13	216	0.513
SRGAP3	0	0	0	0	21	0	0	8	8	216	0.792
SRSF2	0	0	1	1	21	0	0	14	14	216	1.000
SRSF3	0	0	0	0	21	0	0	1	1	216	1.000
SS18	0	0	0	0	21	0	2	3	5	216	1.000
SS18L1	0	0	0	0	21	0	0	22	22	216	0.254
STAG1	0	0	0	0	21	10	2	0	12	216	0.557
STAT3	0	1	0	1	21	1	1	3	5	216	1.000
STAT5B	2	1	0	3	21	1	1	3	5	216	0.023
STAT6	0	0	0	0	21	1	1	3	5	216	1.000
STIL	1	0	0	1	21	0	1	3	4	216	0.928
STRN	1	0	0	1	21	0	1	0	1	216	0.420
SUFU	0	0	0	0	21	0	0	3	3	216	1.000
SUZ12	0	0	0	0	21	0	3	3	6	216	0.963
SYK	0	0	0	0	21	0	1	1	2	216	1.000
TAF15	0	0	0	0	21	0	1	2	3	216	1.000
TAL1	1	0	0	1	21	0	0	3	3	216	0.796
TAL2	0	0	0	0	21	0	0	1	1	216	1.000
TCEA1	0	0	0	0	21	0	1	8	9	216	0.722
TCF12	1	0	0	1	21	3	1	0	4	216	0.928
TCF3	1	0	0	1	21	0	3	4	7	216	1.000
TCF7L2	2	0	0	2	21	3	1	0	4	216	0.159
TCL1A	0	0	0	0	21	0	1	3	4	216	1.000
TEC	0	0	0	0	21	1	3	0	4	216	1.000
TERT	1	0	0	1	21	2	1	6	9	216	1.000
TET1	0	0	0	0	21	7	9	2	18	216	0.345
TFEB	0	0	0	0	21	0	0	7	7	216	0.871
TFG	0	0	0	0	21	2	2	10	14	216	0.473
TFPT	1	0	1	2	21	0	2	10	12	216	0.801
TFRC	1	0	0	1	21	1	1	1	3	216	0.796
TGFBR2	0	0	0	0	21	1	1	10	12	216	0.557
THRAP3	0	0	0	0	21	0	0	1	1	216	1.000
TLX3	0	0	0	0	21	0	0	1	1	216	1.000
TMEM127	0	0	0	0	21	0	0	1	1	216	1.000
TMPRSS2	0	1	0	1	21	0	1	0	1	216	0.420
TNC	0	0	0	0	21	5	0	3	8	216	0.792
TNFAIP3	0	0	0	0	21	1	0	7	8	216	0.792
TNFRSF14	1	0	0	1	21	0	2	4	6	216	1.000
TNFRSF17	1	0	0	1	21	0	1	1	2	216	0.632
TOP1	0	0	0	0	21	2	2	4	8	216	0.792
TP63	0	0	0	0	21	1	0	10	11	216	0.606
TPM3	1	0	1	2	21	1	0	9	10	216	0.649
TPM4	0	0	0	0	21	0	2	3	5	216	1.000
TPR	2	0	1	3	21	5	2	31	38	216	0.936
TRAF7	0	0	0	0	21	0	0	15	15	216	0.436
TRIM24	0	0	0	0	21	1	0	1	2	216	1.000
TRIM27	0	0	0	0	21	0	0	1	1	216	1.000
TRIM33	1	0	0	1	21	2	0	2	4	216	0.928
TRIP11	1	0	0	1	21	3	2	2	7	216	1.000
TSC1	0	0	0	0	21	5	2	1	8	216	0.792
TSC2	0	0	0	0	21	6	0	15	21	216	0.274
TSHR	0	0	0	0	21	3	1	2	6	216	0.963
U2AF1	0	1	2	3	21	0	0	1	1	216	0.000
UBR5	1	0	4	5	21	4	0	23	27	216	0.266
USP44	0	0	1	1	21	0	0	1	1	216	0.420
USP6	1	0	0	1	21	0	1	0	1	216	0.420
USP8	0	0	0	0	21	1	4	1	6	216	0.963
VAV1	0	0	0	0	21	1	3	5	9	216	0.722
VHL	0	0	0	0	21	0	1	6	7	216	0.871
VTI1A	0	0	0	0	21	0	1	0	1	216	1.000
WIF1	0	0	1	1	21	1	0	8	9	216	1.000
WNK2	1	0	0	1	21	0	0	1	1	216	0.420
WRN	1	3	0	4	21	0	4	3	7	216	0.006
WT1	0	0	1	1	21	1	1	11	13	216	1.000
WWTR1	0	0	0	0	21	1	1	4	6	216	0.963
XPA	0	0	0	0	21	0	1	0	1	216	1.000
XPC	0	0	0	0	21	0	0	6	6	216	0.963
XPO1	1	0	0	1	21	2	4	1	7	216	1.000
YWHAE	0	0	0	0	21	1	2	1	4	216	1.000
ZBTB16	1	1	0	2	21	0	1	1	2	216	0.042
ZCCHC8	1	0	0	1	21	0	5	1	6	216	1.000
ZEB1	0	0	0	0	21	2	2	6	10	216	0.661
ZFHX3	0	0	0	0	21	4	0	1	5	216	1.000
ZNF331	0	0	1	1	21	2	3	5	10	216	1.000
ZNF384	0	0	0	0	21	0	0	4	4	216	1.000
ZNF429	0	0	1	1	21	3	1	3	7	216	1.000
ZNF479	0	0	0	0	21	0	1	2	3	216	1.000
ZNF521	0	0	0	0	21	2	2	5	9	216	0.722
ZNRF3	0	0	0	0	21	2	0	4	6	216	0.963

BCLM,breast cancer leptomeningeal metastasis; MBC, non-BCLM metastatic breast cancer cohort;